University of Alberta
Department of Civil Engineering

Structural Engineering Report No. 103

Local Buckling of Thin-Walled Tubular Steel Members

by

M. J. Stephens

G. L. Kulak

and

C. J. Montgomery

February, 1982

LOCAL BUCKLING OF THIN-WALLED TUBULAR STEEL MEMBERS

by

M.J. Stephens

G.L. Kulak

and

C.J. Montgomery

DEPARTMENT OF CIVIL ENGINEERING

THE UNIVERSITY OF ALBERTA

EDMONTON, ALBERTA

February, 1982

ABSTRACT

The local buckling of thin-walled fabricated steel cylinders loaded in uniform axial compression or pure flexure is investigated. Existing design specifications give empirical local buckling ultimate strength equations that make no distinction between a flexural or compressive failure. These equations are based on a small body of widely scattered test results for fabricated steel tubes, none of which involve flexurally loaded specimens. An experimental program was, therefore, undertaken to examine the difference in behavior between the two load cases.

The testing program involved a preliminary series of small-scale compression tests, and two large diameter series of matched bending and compression tests. Relative buckling strengths are compared and the effects of fabrication induced imperfections on the proportional limit and ultimate buckling strength are assessed. Test results obtained herein are compared with the experimental results of others, and with predicted results as determined from the available design formulas.

On the basis of the limited amount of test evidence for flexurally loaded fabricated cylinders, the assumed equivalence between the compressive and flexural buckling strengths is justified. Evaluation of the existing data indicates that design formulas are available which adequately predict the behavior of fabricated cylinders loaded in either compression or bending. An alternate local

buckling ultimate strength equation is presented which simplifies the design procedure, and is shown to normalize the test results over a wider range of material yield strengths when compared with existing formulas.

Further experimental study is required to establish conclusively the flexural buckling strength of fabricated steel tubes. Additional testing is also recommended to determine the effects of welding induced imperfections on the buckling strength of tubular members with wall thicknesses less than about 6 mm.

ACKNOWLEDGEMENTS

This report is based on the thesis submitted by Mark James Stephens to the Faculty of Graduate Studies and Research at the University of Alberta in partial fulfillment of the requirements for the degree of Master of Science in Civil Engineering.

The authors thank Larry Burden and Richard Helfrich for their advice and assistance during the experimental phase of the program, and Tom Casey for his help in computer-related areas.

TABLE OF CONTENTS

LIST OF TABLES

LIST OF FIGURES

Figure

Page

NOTATION

a_o = normalized imperfection amplitude

b = equivalent plate width

C = compression buckling coefficient for a thin-walled cylinder

C_γ = proposed compression buckling coefficient for a thin-walled cylinder

D_{max} = maximum inside diameter of a thin-walled cylinder

D_{min} = minimum inside diameter of a thin-walled cylinder

E = elastic modulus

E_s = secant modulus

E_t = tangent modulus

k = buckling coefficient for a flat plate

L = cylinder length

l_r = gage length for imperfection amplitude measurements

O_r = cylinder out-of-roundness

q = plate width coefficient

R = cylinder radius

s = number of radii measurements per specimen

t = cylinder wall thickness or plate thickness

U = unevenness factor

α = general capacity reduction factor

α_o = capacity reduction factor for uniform axial compression

α_b = capacity reduction factor for pure flexure

α_m = capacity reduction factor for uniform axial compression and pure flexure

β = general capacity reduction factor for fabricated cylinders

γ = proposed nondimensional buckling parameter

γ_s = proposed nondimensional buckling parameter incorporating the static yield stress

Δ = nondimensional buckling parameter

η = plasticity reduction factor

ν = elastic Poisson's ratio

ρ = nondimensional buckling parameter

σ_{br} = Brazier buckling stress of a thin-walled cylinder

σ_{cl} = classical elastic buckling stress of a thin-walled cylinder

σ_{el} = classical elastic buckling stress of a flat plate

σ_p = proportional limit

σ_u = ultimate buckling stress of a thin-walled cylinder

σ_y = yield stress

σ_{yd} = dynamic yield stress

σ_{ys} = static yield stress

ω_o = imperfection amplitude

ω_o' = asymmetric imperfection amplitude

ω_o'' = axisymmetric imperfection amplitude

1. INTRODUCTION

1.1 Thin-Walled Tubular Members

Thin-walled tubular members fabricated from steel plate are used extensively in civil engineering structures. Columns, stacks, conveyor support systems, and other such stuctures are often constructed of unstiffened panels or discretely stiffened panels which behave in an essentially unstiffened manner.

This report deals, in part, with the local buckling strength of thin-walled unstiffened tubular members subjected to flexural loads. Since the behavior of tubular members subjected to uniform axial compression is closely related to the behavior under flexural loads, the more fundamental axial compression load case is also considered.

The experimental phase of the study will focus on the type of tubular member that is used extensively in the materials-handling operations of industrial plants. These are fabricated circular steel cylinders, typically 2.4 m to 4 m in diameter, with radius-to-thickness ratios in the range of 150 to 400. They support and enclose conveyor systems and customarily span distances up to about 50 m.

In the design of these long-span tubular members, moment capacity is usually found to govern the member strength. The moment capacity is controlled by either material yielding or local buckling of the cylinder wall.

Lateral torsional buckling of the member is unlikely because of the inherently large torsional and lateral resistance provided by the circular shape of the cross-section. Because large radius-to-thickness ratios are employed, local buckling often precludes the attainment of the yield moment and, depending on the stress level at the point of instability, either elastic or inelastic buckling behavior is possible.

Although circumferential ring stiffeners are often employed to maintain the circular shape of the member cross-section during loading, the stiffener spacings commonly used do not increase the local buckling strength. As a result, these members are considered to be unstiffened for purposes of design.

1.2 Statement of Problem

Criteria for the design of thin-walled fabricated structural members are presented in a variety of North American specifications. For tubular members, the design recommendations are based on empirical local buckling strength equations established from tests on cylinders made from sharp-yielding mild steels.

Current specifications do not distinguish between the local buckling strength of cylindrical members subjected to uniform axial compression and the flexural strength of these members. This lack of distinction arises from an inadequate

data base for flexurally loaded tubular steel members. Even for the case of axial compression, test results show a large amount of scatter and there is no unified theory to explain the observed experimental behavior. Consequently, there exists a large element of uncertainty in the prediction of local buckling strengths for thin-walled tubular members fabricated from mild steel plate.

1.3 Objectives

The objectives of this study are:

1. To test, in both axial compression and pure flexure, large diameter fabricated steel cylinders with radius-to-thickness ratios between the limits of 149 and 222.
2. To compare test results with theoretically based predictions and, where applicable, with previously obtained test results on similar specimens.
3. To establish the validity of presently available design procedures as they apply to axially compressed and flexurally loaded fabricated cylinders.
4. To develop an alternate local buckling ultimate strength equation suitable for design applications.
5. To make recommendations for future testing.

2. REVIEW OF LOCAL BUCKLING BEHAVIOR

2.1 Introduction

In this chapter, the analytical solutions to the problems of elastic and inelastic local buckling of axially loaded and flexurally loaded cylinders are presented. First, the classical linear solutions are given for the case of a geometrically perfect cylinder, and the implications of the more refined nonlinear analyses are discussed. Next, the effects of both geometric and material imperfections on the buckling capacity are considered. Finally, some of the existing design specifications applicable to thin-walled fabricated steel cylinders are reviewed.

2.2 Instability of Tubular Members

Buckling is a form of instability that can lead to collapse of a structure under loads that are less than those normally required to cause material failure. Thin-walled unstiffened tubular members, and other such shell-like members, are susceptible to this type of failure. Depending on the member geometry and loading conditions, instability of only a portion of the cylinder wall may occur before the member as a whole becomes unstable. This form of instability is referred to as local buckling.

To better understand the problems associated with a local buckling stability analysis of bent and compressed

cylinders, a brief description of the ways in which a member becomes unstable is in order.

Irrespective of the mode of failure, in the early stages of loading a geometrically perfect member is in a prebuckled or fundamental state of equilibrium characterized by a single primary path on a load-displacement plot (See Fig. 2.1). As the load increases, it is possible that the member will reach a critical state corresponding to a bifurcation point. At this point there exists more than one physically admissible equilibrium state. The primary path continues beyond the bifurcation point but equilibrium is unstable in this region. In a real structure, when the bifurcation or buckling load is reached, the member goes into a buckled equilibrium configuration represented by a secondary path branching from the primary path (Fig. 2.1a). Because of the relatively small deflections involved, a theory based on infinitesimal displacements is usually adequate to predict the behavior up to and including the bifurcation point.

Should the primary equilibrium path reach a relative maximum before a secondary path is intersected, this relative maximum is known as a limit point, and the corresponding load is known as the limit load (Fig. 2.1b). In contrast to the infinitesimal displacements associated with bifurcation, when the member buckles at the limit load there is a sudden transition, involving finite displacements, from an unstable to a stable configuration.

If the behavior of the member beyond the bifurcation point or limit point is of interest, a postbuckling theory based on finite displacements is required to trace the load-displacement path. This is necessary because small-displacement theories do not provide any indication of the behavior in the postbuckled region.

When the member under consideration contains imperfections, theories based on the assumption of an initially perfect configuration are no longer correct. Specifically, for thin-walled cylinders, the unstable nature of their initial buckled state makes them extremely sensitive to disturbances which cause a premature transition from the prebuckled to the postbuckled state. In real structures, such disturbances are usually caused by initial geometric imperfections. Thin-walled cylindrical members are therefore imperfection sensitive and theories that attempt to predict their buckling strength should take into account their imperfections.

2.3 Small-Displacement Theory

The simplest approach to the thin-walled cylinder stability problem is to consider a geometrically perfect member, elastic material behavior, and linear relationships between displacements, strains, and curvatures. This so-called classical stability approach is based on the assumption of infinitesimal displacements and therefore

precludes consideration of finite initial geometric imperfections. Because all nonlinear terms are excluded from the derivation, the classical stability theory is often referred to as a linear or small-displacement stability theory.

2.3.1 Axial Compression

The classical approach to the local buckling of unstiffened cylindrical shells under the action of uniform axial compression was first undertaken in an approximate form by Lorenz (1) in 1908. In succeeding years the analysis was generalized and refined by Timoshenko (2), Southwell (3), Flügge (4), and Donnell (5), leading to a unified solution for both local and overall elastic buckling of compressed cylinders.

As a result of the work cited above, the elastic buckling loads, and the corresponding buckled shapes can be shown to depend upon both dimensional parameters—length(L), radius(R), and thickness(t)—and material properties—modulus of elasticity(E) and Poisson's ratio(ν). Neglecting unimportant terms in the general solution, three distinct regions of behavior can be distinguished:

1. Short cylinders ($L/R < 1.72(t/R)^{1/2}$); those which buckle in a manner similar to that of axially compressed flat plates (See Fig.2.2a).
2. Long cylinders ($L/R > 2.85(R/t)^{1/2}$); those which fail as long columns through overall instability prior to

local buckling (Fig. 2.2b).

3. Moderate-length cylinders which fall between the above slenderness limits, and which buckle locally in either an axisymmetric mode (Fig. 2.2c) or an asymmetric mode (Fig. 2.2d). The latter form grows into the characteristic depressed-diamond shape (Fig. 2.2e) under continued deformation in the buckled state.

Of the three types of behavior described, only the local buckling behavior of moderate-length cylinders is dealt with in this report.

The critical axial stress for members of intermediate slenderness is length independent and identical for both local buckling modes. For a cylinder with simply supported edges the classical buckling stress is (6)

$$\sigma_{cl} = CE\frac{t}{R} \qquad (2.1)$$

where

$$C = \frac{1}{[3(1-\nu^2)]^{1/2}}$$

$$= 0.605 \quad \text{for } \nu = 0.3$$

In the moderate-length to long cylinder transition region, however, buckling mode interaction can have a pronounced detrimental effect on the critical stress. Prior to the transition from local to overall buckling which occurs at $L/R \cong 2.85(R/t)^{1/2}$, there exists the possibility

that the asymmetric local buckling mode will couple with the overall column buckling mode resulting in a critical stress as low as 60% of the classical value as determined from Eq. 2.1. Esslinger *et al.* (7) have suggested that for simply supported tubes this interaction is possible when $L/R > 0.95(R/t)^{1/2}$. Despite this observation, the transition behavior is often ignored because there are other factors (to be discussed later) which have a greater influence on actual performance and which often preclude this mode interaction.

From the preceding discussion, it is important to note the limits of applicability of the theory of local buckling for moderate-length cylinders. For cylinders of the type considered in this study ($R/t \cong 200$), the length-independent local buckling mode governs for $0.122 \leq L/R \leq 40.3$. The comparatively great range of cylinder lengths encompassed by this theory make it applicable to a wide variety of civil engineering structures.

2.3.2 Flexure

The classical solution for local buckling induced by pure flexure is usually attributed to Flügge (4). In 1932, he performed an approximate calculation using linear elastic stability theory, and assuming a particular buckle wavelength-to-radius ratio. His analysis showed a 30% increase in bend buckling capacity over the classical axial load value (Eq. 2.1). This calculation was cited by

Timoshenko (8) without a qualifying statement as to assumed buckle wavelength and has been used as a general rule ever since. Flügge's calculations were supported by early experimental evidence which showed an increase in buckling capacity for flexure which often exceeded the assumed value of 1.3 times the compression value.

In 1961, Seide and Weingarten (9) performed a numerical small-displacement analysis of the flexural case which indicated that the critical wavelength assumed by Flügge was incorrect. The results showed that the flexural buckling stress is approximately equal to the compressive buckling stress. This removed small-displacement theory as a basis for any difference between the critical bifurcation buckling stress in bending and compression.

Unlike uniformly compressed cylinders, however, there exists a limit point buckling mode for flexurally loaded tubes which is distinct from the bifurcation-type buckling mode discussed in Section 2.3.1. This mode of failure was first investigated by Brazier (10) in 1927 ("The Brazier Effect").

If a long cylindrical tube is subjected to a bending moment it will assume a curvature. Because of this bending induced curvature, the longitudinal tension and compression stresses will have components directed towards the mid-plane of the tube. The effect of these components is to squeeze the tube into an oval shape, thereby reducing its resistance to bending. By applying a small-displacement theory to a

tube of infinite length, Brazier determined the limit point moment. If the longitudinal bending stress is based on the geometry of the undeformed cross-section, this moment corresponds to a maximum axial stress of

$$\sigma_{br} = \frac{2}{9}\left[\frac{2}{(1-\nu^2)}\right]^{1/2} E\,\frac{t}{R} \qquad (2.2)$$

$$= 0.329\,E\,\frac{t}{R} \quad \text{for } \nu = 0.3$$

which is approximately one-half the classical compression buckling stress.

In addition, this tendency for the cross-section of a tube in bending to become oval leads to the possibility that bifurcation could occur at a reduced moment after considerable ovaling has taken place. The flattening of the cross-section would result in relatively larger stresses for a given moment, and the critical bifurcation buckling stress would be lower because of the increase in the local radius of curvature at the point of maximum stress.

This problem of bifurcation-type buckling from an initially oval state was first considered by Aksel'rad (11) in 1965, and his approximate results have been verified by Stephens *et al.* (12). Aksel'rad's analysis indicates that the buckling stress for tubes of finite length varies from the classical buckling stress of 0.605 Et/R for short cylinders, to slightly less than the Brazier stress, 0.295 Et/R, for long cylinders ($L/R > 2.5(R/t)^{1/2}$).

If a bent cylinder is restrained against significant ovaling by discrete bulkheads, or circumferential ring-stiffeners, then Brazier-type buckling will be prevented and mode interaction between ovaling and bifurcation will have a negligible effect. Tubular members so restrained can therefore be analysed by considering only bifurcation-type buckling of the undeformed circular cross-section.

2.3.3 Comments on Inelastic Material Behavior

When the buckling stress is below the proportional limit of the material, the assumption of elastic material behavior is valid. If the stresses are above the proportional limit, the modulus of the material becomes a function of the stress level. In the inelastic range, the material modulus decreases causing a decrease in the stiffness of the member and a corresponding reduction in buckling strength.

For inelastic local buckling, the NASA shell stability design guide (13) recommends that the elastic modulus, E, be multiplied by a plasticity reduction factor, η, to reflect the variation in material stiffness with the stress level. The recommended plasticity reduction factor is

$$\eta = \frac{(E_s E_t)^{1/2}}{E} \tag{2.3}$$

where E_s and E_t are the secant and tangent modulii, respectively.

Equation 2.3 is a simplified form of the theoretical plasticity reduction factor suggested by Gerard (14). It is intended to apply to homogeneous materials with gradual-yielding stress-strain curves. For cylinders fabricated by welding from sharp-yielding steels, the previously defined plasticity reduction factor is not directly applicable. Residual stresses, introduced during fabrication, result in nonhomogeneous material behavior wherein localized regions of the cylinder deform plastically before the nominal member stress reaches the yield point. Theoretically based reduction factors do not account for this type of behavior. Plasticity reduction factors for structural steels are, therefore, usually determined empirically.

2.4 Large-Displacement Theory

2.4.1 Axial Compression

Experiments performed to verify the theoretical results of the classical shell stability theory have shown that, in contrast to experience gained with other slender structural elements such as plates and columns, the actual buckling loads of thin-walled cylinders are appreciably different from the buckling loads predicted by linear theory. For the case of axially loaded cylinders the difference is very large; test results often average only about 1/2 to 1/3 of the classical value. In addition to lack of agreement with

predictions, the test results show unusually large scatter. In all cases the scatter exceeds by far that associated with tests on slender columns and plates.

Initially the discrepancy between theory and experiment was attributed to test specimen end effects. Refinement of the linear shell buckling theories to account for these effects (15,16) has shown, however, that boundary conditions have relatively little effect on the buckling load of moderate-length cylinders with practical support conditions.

Important progress towards better understanding of the buckling behavior of compressed cylinders was achieved in 1941 by von Kármán and Tsien (17). Their approximate numerical analysis, based on the elastic nonlinear finite-displacement theory developed by Donnell (5), enabled them to show that the asymmetric or diamond-shaped buckling configuration is unstable. Specifically, the results indicate that equilibrium states involving large displacements can be maintained by loads far less than the critical bifurcation load obtained from classical small-displacement theory.

This buckling instability accounts for the difference between the behavior of compressed cylinders and that of columns and edge-supported flat plates. Qualitatively, the difference can be attributed to the nature of the transverse membrane stresses that develop after buckling starts. A flat plate develops significant transverse tension membrane stresses after buckling because of restraint provided by

support along the unloaded edges (Fig. 2.3a). These membrane stresses act to restrain lateral motion and the plate can therefore carry additional load after buckling. A column, after buckling, develops no significant transverse membrane stresses to restrain lateral motion and is free to deflect laterally at the critical buckling load (Fig. 2.3b). During the course of buckling, the load sustained by the column does not drop off. For a thin cylinder, the inward buckling of the asymmetric diamond-shaped mode generates superimposed transverse compression membrane stresses (Fig. 2.3c), and the initial buckled form is therefore unstable. Consequently, buckling is coincident with failure and is followed by a considerable drop in the load carrying capacity of the cylinder. The various types of postbuckling behavior are illustrated in Fig. 2.4.

With the realization that cylindrical shells under axial compression possess an initially unstable buckled configuration, there was theoretical justification for the experimentally observed tendency towards imperfection sensitivity. In 1945, Koiter (18) incorporated finite initial imperfections into his general nonlinear stability theory.

Koiter's theory permits the determination of a maximum load that can be maintained before buckling is triggered, and relates this load to the size of the imperfection which causes the premature buckling. In general, the larger the initial imperfection the smaller the buckling load.

The inclusion of initial imperfections, in addition to providing a path for the transition from the unbuckled to the buckled state at loads less than the classical value (See Fig. 2.4), also helps to account for the large amount of scatter observed in the test results. Because of the statistically random nature of initial imperfection amplitudes, some variation in buckling load would be expected. Furthermore, recalling that two critical bifurcation mode shapes are possible for local buckling (Section 2.3.1), the sensitivity to imperfections inherent in the unstable asymmetric buckling mode accounts for its predominant occurrence in experiments. The stable, and therefore relatively insensitive axisymmetric buckling mode, can only be induced at or near the classical buckling stress.

In his derivation, Koiter initially assumed that the imperfections were axisymmetric in shape. The basic axisymmetric imperfection theory was subsequently modified and extended by Almroth (19) and by Tennyson and Muggeridge (20). In the latter study, tests were performed on cylinders with axisymmetric imperfections carefully machined into the wall. Good correlation between theory and experiment was obtained. However, further investigation by Koiter (21) into the effects of imperfection shape on the buckling load has shown that interaction between various axisymmetric and asymmetric modes results in a more pronounced reduction in strength.

The effects on the buckling load, of Koiter's assumed three-mode imperfection shape, and the earlier single mode imperfection shape, are shown in Fig. 2.5 as a function of imperfection amplitude. The nondimensional imperfection amplitude, a_o, is the absolute imperfection amplitude, ω_o, normalized with respect to the wall thickness. The reduction in buckling stress is expressed by a capacity reduction factor, α, which is the actual buckling stress divided by the classical buckling stress.

More recent study of the effects of imperfections on the buckling strength, as discussed in review articles by Arbocz (22) and Babcock (23), involves the use of more accurate numerical techniques applied to single and multiple mode imperfection shapes and to statistically random imperfection amplitudes. The analyses have progressed to the point where considerable success can be achieved in predicting the elastic buckling loads of test specimens, provided that the actual imperfection profiles are mapped and used in the calculation.

With respect to fabricated cylinders made from sharp-yielding steels, such analysis procedures are rendered less reliable by the existence of residual stresses due to cold forming and welding, and by inelastic material behavior. Neither of these effects have been incorporated into the numerical analysis procedures currently available.

2.4.2 Flexure

The analysis of cylindrical shells in bending has not advanced as far as has the analysis for axially loaded cylinders. Although classical small-displacement theory gives approximately the same buckling stress for both compression and bending, experimental results indicate a higher buckling stress for flexurally loaded members. No large-displacement bifurcation-type buckling analysis exists to show whether or not the increase in strength is an inherent characteristic of cylinders in bending. In place of theory there is conjecture as to the possible reasons for the difference in behavior.

The experimental buckle patterns for cylinders in bending are much like those obtained for axial compression. It is therefore assumed that the theoretical buckling behavior under both loading conditions is similar and that imperfections are significant for both. The stress distribution varies circumferentially in the case of bending, however, so that the shell has a preferred region of buckling. The lower probability of imperfections occurring within this region could result, on average, in higher buckling stresses in bending than in compression. Still, it would be expected that some bend buckling stresses would approach the corresponding compression values. As illustrated by Fig. 2.6, this has not been shown to be the case. A pronounced increase in flexural buckling strength relative to compression buckling strength is indicated and

is shown to be a function of R/t. This curve was established using the lower bound best-fit curves through the available test results as established by Weingarten *et al.* (24) in their review of aerospace quality specimens that buckled elastically. It is generally believed that the strain gradient resulting from the circumferentially varying bending stress is responsible for this increase in buckling strength.

2.5 Design Procedures

2.5.1 Type of Member Considered

As discussed previously, the buckling behavior of thin-walled cylinders is considerably affected by imperfections, both in the material and in the geometry. It is therefore convenient for design to classify steel tubes into groups with similar imperfection levels and consequent buckling behavior.

Tubes produced by a hot forming process in a plant devoted specifically to the production of tubes are classified as manufactured tubes. Cylinders made by cold forming from steel plate, and joined by riveting, bolting, or welding in an ordinary structural fabrication shop are fabricated tubes.

Fabricated tubes have been distinguished from manufactured tubes because test results indicate that their

local buckling strength may be considerably below that of manufactured tubes. This is apparently the result of larger geometric imperfections and the presence of residual stresses introduced during cold forming and subsequent welding.

This investigation deals specifically with the behavior of fabricated tubular members. Emphasis is therefore placed on design procedures that take into account the increased levels of geometric and material imperfection.

2.5.2 Ultimate Strength Formulas

The Canadian Standards Association (CSA) presents requirements for fabricated tubular members in CSA Standard S136-1974, "Cold Formed Steel Structural Members" (25). This Standard is based on the 1980 edition of the American Iron and Steel Institute (AISI) light gage steel specification (26). The latter specification presents a local buckling ultimate strength curve for axially loaded cylinders made from sharp-yielding steels which simultaneously accounts for nonhomogeneous inelastic material behavior and initial imperfections. This empirical equation and other similar equations are shown in Fig. 2.7 together with the test results obtained by Wilson (27) and Wilson and Newmark (28) on fabricated tubes of moderate-length ($1.72(t/R)^{1/2} \leq L/R \leq 2.85(R/t)^{1/2}$). The following discussion takes a form similar to that used by Johnston (29).

The empirical equations shown incorporate a nondimensional relationship first reported by Plantema (30) in 1946. In deriving an empirical formula for manufactured tubes he found that the ratio between the ultimate buckling stress and the yield stress (σ_u/σ_y) depends on the buckling parameter

$$\rho = \frac{Et}{\sigma_y R} \tag{2.4}$$

which is a measure of the ratio between the classical elastic buckling stress (Eq. 2.1) and the material yield stress. The Plantema formula is

$$\frac{\sigma_u}{\sigma_y} = 0.166\rho \qquad \text{for } \rho \leq 5 \tag{2.5a}$$

$$\frac{\sigma_u}{\sigma_y} = 0.75 + 0.016\rho \qquad \text{for } 5 < \rho < 16 \tag{2.5b}$$

$$\frac{\sigma_u}{\sigma_y} = 1.0 \qquad \text{for } \rho \geq 16 \tag{2.5c}$$

The transition between linear elastic behavior (Eq. 2.5a), and yielding (Eq. 2.5c), consists of a straight-line approximation (Eq. 2.5b) which intersects the elastic curve at a proportional limit of 83% of σ_y (Point A in Fig. 2.7).

The Plantema formula was conservatively modified by the AISI (26) on the basis of the test results shown in Fig. 2.7 to make it more applicable to fabricated tubes. This involved reducing the predicted ultimate buckling strength

in the inelastic region of behavior. The resulting AISI formula is

$$\frac{\sigma_u}{\sigma_y} = 0.665 + 0.0187\rho \qquad \text{for } 4.55 < \rho < 17.9 \qquad (2.6a)$$

$$\frac{\sigma_u}{\sigma_y} = 1.0 \qquad \text{for } \rho \geq 17.9 \qquad (2.6b)$$

Equation 2.6a intersects Plantema's elastic buckling stength equation at $\rho = 4.55$ ($R/t = 44800/\sigma_y$) which implies a reduced proportional limit for fabricated tubes of 75% of σ_y (Point B in Fiq. 2.7). No recommendation is made for cylinders with $R/t > 44800/\sigma_y$ on the basis that elastic buckling involves geometries outside the range typically encountered in fabricated steel tubes.

The American Water Works Association (AWWA) standard (31) gives a parabolic equation for the local buckling strength that does not distinguish between elastic and inelastic buckling and, unlike the AISI formula, applies to cylinders in the so-called elastic region of behavior.

This strength formula

$$\frac{\sigma_u}{\sigma_y} = 0.138\rho - 0.00475\rho^2 \qquad \text{for } \rho < 14.5 \qquad (2.7a)$$

$$\frac{\sigma_u}{\sigma_y} = 1.0 \qquad \text{for } \rho \geq 14.5 \qquad (2.7b)$$

is based strictly on test results (27,28) and applies to mild steels with $\sigma_y \geq 200$ MPa and $t \geq 6.35$ mm.

On comparing these design equations it is apparent that the varying interpretations of the widely scattered test data leads to a substantial disagreement between the curves shown. In an attempt to reduce the data scatter, Miller (32) considered a modified form of the nondimensional buckling parameter proposed by Plantema. Miller's parameter is

$$\Delta = \alpha_m C \frac{Et}{\sigma_y R} \tag{2.8}$$

where

$$\alpha_m = -0.041 - 0.473 \log \left(\frac{UR}{t} \right) \tag{2.9}$$

The classical elastic buckling stress CEt/R is modified by a capacity reduction factor, α_m, based on the approximate—and in places intuitively based—imperfection theory of Donnell and Wan (33). Equation 2.9 is a semi-log approximation of their theoretical nondimensional buckling strength curve wherein a relationship between the capacity reduction factor and R/t is defined in terms of an unevenness factor U. This factor reflects the initial level of cylinder wall imperfection (geometric and material), and is considered to be a function of the method of construction. Evaluation of the available test data led Miller to select an unevenness factor of U = 0.0005 for fabricated cylinders.

With imperfections accounted for in this manner, a lower bound curve through the data points represents an empirical equation for the plasticity reduction factor, η, applicable to nonhomogeneous, sharp-yielding mild steels.

Miller's buckling strength formula is

$$\frac{\sigma_u}{\sigma_y} = \eta\alpha_m C \frac{Et}{\sigma_y R} \qquad (2.10)$$

$$= \eta\Delta$$

where

$$\eta = 1.0 \qquad \text{for } \Delta \leq 0.55$$

$$\eta = \frac{0.45}{\Delta} + 0.18 \qquad \text{for } 0.55 < \Delta < 1.6$$

$$\eta = \frac{1.31}{(1+1.15\Delta)} \leq \frac{1}{\Delta} \qquad \text{for } \Delta \geq 1.6$$

A modified form of Miller's formula was adopted by the American Society of Mechanical Engineers (ASME) in 1980 for their specification on "Metal Containment Shell Buckling Design Methods" (34) which forms an appendix to the ASME Boiler and Pressure Vessel Code. Equation 2.9 was modified such that

$$\alpha_m = 0.207 \qquad \text{for } 600 \leq \frac{R}{t} \leq 1000 \qquad (2.11a)$$

$$\left.\begin{aligned} \alpha_m &= 1.52 - 0.473 \log\left(\frac{R}{t}\right) \qquad (2.11b) \\ \alpha_m &= 300\frac{\sigma_y}{E} - 0.033 \qquad (2.11c) \end{aligned}\right\} \text{lesser value} \quad \text{for } \frac{R}{t} < 600$$

The changes were made on a strictly empirical basis to further improve the correlation between predicted and test results. In addition, the ASME code restricts the

applicability of their formula (as defined by Eqs. 2.10 and 2.11) to cylinders with wall thicknesses not less than 6.35 mm.

The ASME formula, together with the test results used to establish the curve (27,28,35,36) are shown in Fig. 2.8. The data points falling significantly below the curve are considered suspect because of reported variations in compressive strain during loading.

None of the buckling strength equations, as presented, take into account the possibility of a reduced buckling load due to coupling between local and overall column buckling for moderately long cylinders. In allowing for this effect, the method used in many steel column specifications involves an interaction approach which is equivalent to substituting the local buckling stress for the yield stress in the appropriate column buckling equation. Using the Column Research Council's column-strength curve (37), and the experimental results obtained by Ross and Chen (36) and Wilson and Newmark (28) for long tubular columns, Miller (32) established a slenderness limit. He recommends that cylinders in which

$$\frac{L}{R} \leq 0.47 \left(\frac{E}{\sigma_u} \right)^{1/2} \qquad (2.12)$$

will buckle locally at a load which is insensitive to column length.

In all of the above mentioned specifications, no distinction is made between compressively-induced and flexurally-induced local buckling. The unanimous recommendation is that the bend buckling capacity be taken equal to the compression buckling capacity. Two factors contribute to this lack of distinction. First, there is a lack of test results for flexurally loaded fabricated tubes which buckle below the yield stress. Second, the results of elastic buckling tests as reviewed by Weingarten *et al.* (24) indicate that the assumed equivalence between flexure and compression is a conservative approach.

The European Convention for Construction Steelwork (ECCS) goes beyond this simplified approach, and in their manual on shell stability (38) permit higher buckling stresses in bending than in compression. This recommendation, though not yet substantiated by theory, is none the less supported by a substantial data base for small-scale cylinders failing elastically in either compression or flexure (24).

The basis for the ECCS approach is the application of an empirical capacity reduction factor to the classical buckling stress, followed by a further empirically based reduction to account for inelastic behavior and residual stress effects should the elastic buckling stress exceed the assumed proportional limit of 50% of σ_y.

The capacity reduction factors, α_o for compression, and α_b for bending, suggested by the ECCS are

$$\alpha_o = \frac{0.83}{[1+R/(100t)]^{1/2}} \quad \text{for } \frac{R}{t} > 212 \tag{2.13a}$$

$$\alpha_o = \frac{0.70}{[0.1+R/(100t)]^{1/2}} \quad \text{for } \frac{R}{t} \leq 212 \tag{2.13b}$$

and

$$\alpha_b = 0.1887 + 0.8113\alpha_o \tag{2.13c}$$

Both factors are based on simplified forms of the lower bound best-fit curves established by Weingarten *et al.* (24) for aerospace applications.

The ECCS formula for the buckling capacity of fabricated steel cylinders is

$$\frac{\sigma_u}{\sigma_y} = \frac{\alpha}{\beta} C \frac{Et}{\sigma_y R} \quad \text{for } \alpha C E \frac{t}{R} \leq \frac{\sigma_y}{2} \tag{2.14a}$$

where

$$\beta = \frac{4}{3}$$

and

$$\frac{\sigma_u}{\sigma_y} = 1 - 0.4123 \left[\frac{\sigma_y}{\alpha C E (t/R)} \right]^{0.6} \quad \text{for } \alpha C E \frac{t}{R} > \frac{\sigma_y}{2} \tag{2.14b}$$

In either equation α is taken as α_o for compressive loading, and α_b for flexural loading.

In qualifying the use of the above equations the ECCS has recognized that, in general, results based on specimens made to the close tolerances of the aerospace industry could

not be considered directly applicable to fabricated structural steel cylinders. This reasoning led to the inclusion of the β term in the elastic buckling equation (Eq. 2.14a) which reduces the expected stress to 75% of the value predicted for aerospace quality specimens. Furthermore, there is a restriction on permissible geometric imperfection size such that

$$\omega_0 \leq \frac{(Rt)^{1/2}}{25} \tag{2.15}$$

measured from a straight rod of length $l_r = 4(Rt)^{1/2}$. For cylinders with imperfections twice this size the α term is reduced by one-half and for imperfection amplitudes between $(Rt)^{1/2}/25$ and the upper limit of $2(Rt)^{1/2}/25$, linear interpolation is permitted.

Because the above procedure is applicable only to local buckling, a restriction on cylinder length is imposed beyond which the member slenderness may undermine the buckling strength. The length limitation is

$$\frac{L}{R} \leq 0.95 \left(\frac{R}{t}\right)^{1/2} \tag{2.16}$$

This is based on the theoretical work of Esslinger *et al.* (7) as discussed in Section 2.3.1.

2.6 Summary

Axially loaded and flexurally loaded tubular members have practically identical bifurcation buckling stresses according to classical stability theory. Cylinders in bending are, in addition, susceptible to a form of limit point buckling characterized by flattening of the cross-section. This type of instability, however, does not develop in members which are restrained against significant ovaling at discrete intervals by either rigid bulkheads or ring stiffeners.

Inelastic material behavior can be accounted for by incorporating a plasticity reduction factor to reflect the material's reduction in stiffness with increasing stress level. Homogeneous, gradual-yielding materials can be handled by a theoretically based plasticity reduction factor, whereas nonhomogeneous, sharp-yielding materials are dealt with using empirical plasticity reduction factors.

In realistic cylindrical structures, imperfection sensitivity, caused by an unstable buckled configuration, results in an actual buckling stress considerably below the classical buckling stress. Finite-displacement stability theories are available which can account for the effects of initial geometric imperfections. Numerical analysis techniques, based on these theories, can accurately predict the elastic buckling stress, provided that the imperfection profiles of the cylinder in question are mapped and used in the calculation.

The requirement of complete mapping of each specimens individual imperfection spectrum, and the inability of the numerical procedures to account for nonhomogeneous inelastic material behavior, lead to the conclusion that further investigation is required before the results of this type of analysis can be applied by the design engineer in a practical sense. Alternatively, empirical local buckling ultimate strength equations are available for cylinders fabricated from mild structural steels. These equations simultaneously account for imperfections and nonhomogeneous inelastic material behavior.

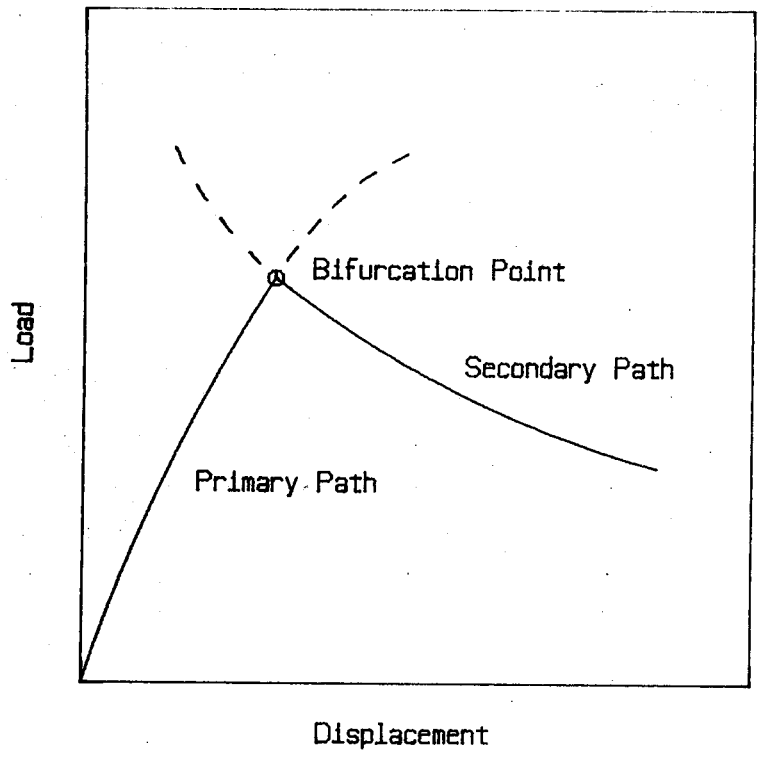

(a)

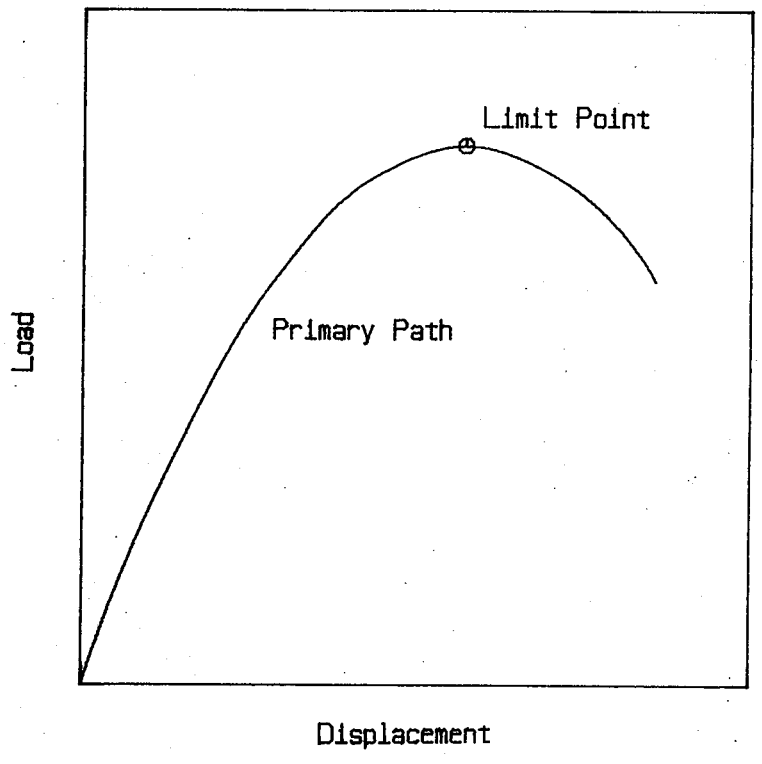

(b)

Figure 2.1 Generalized Load-Displacement Behavior

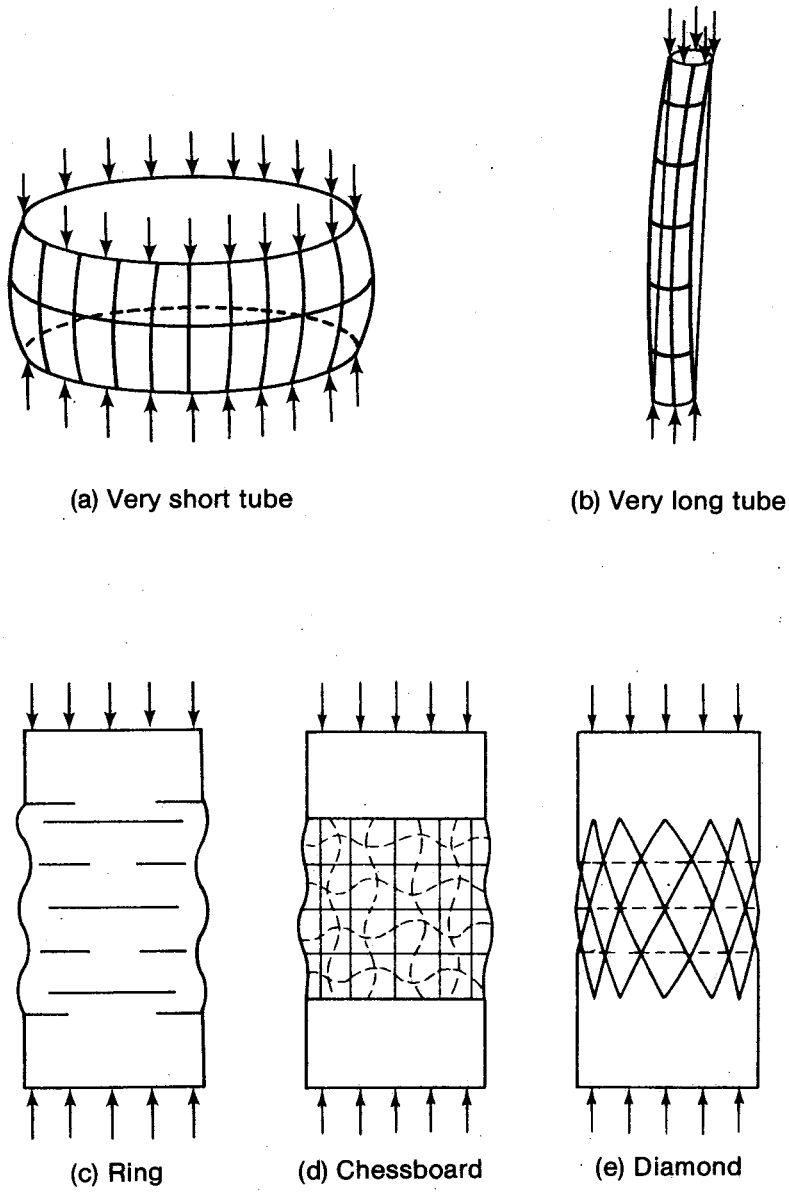

Figure 2.2 Buckling Modes for Thin-Walled Cylinders

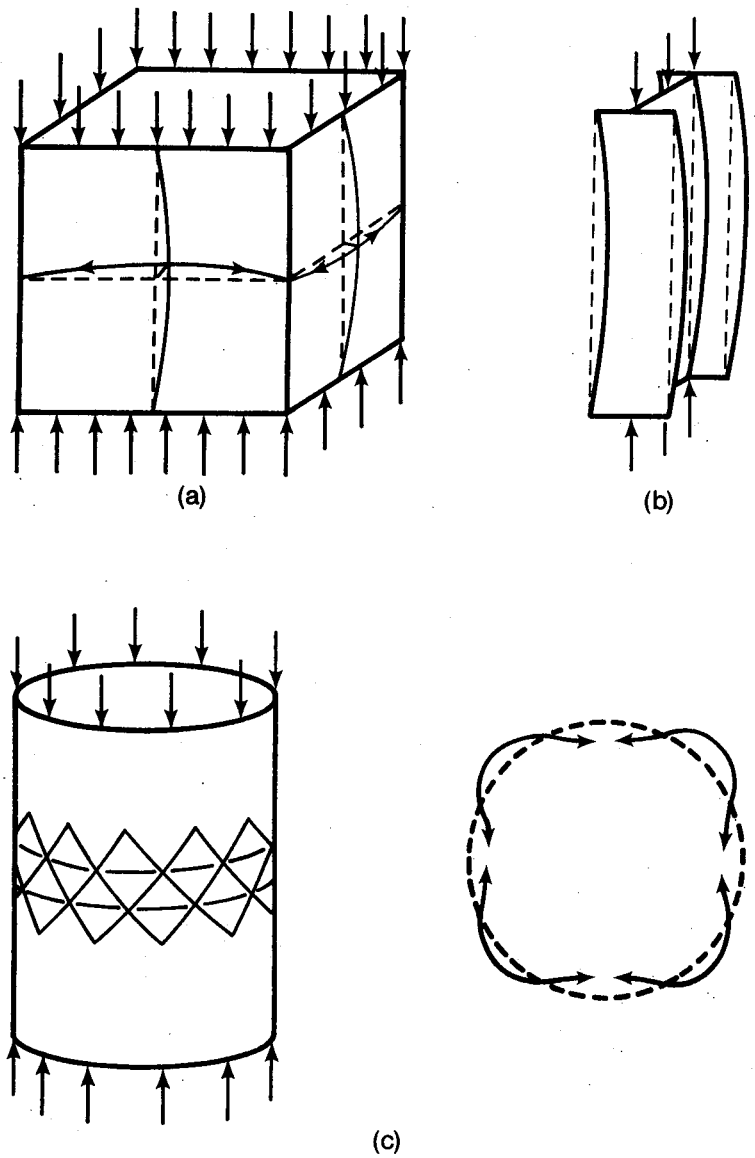

Figure 2.3 Transverse Membrane Stresses in Flat Plates, Columns, and Thin-Walled Cylinders

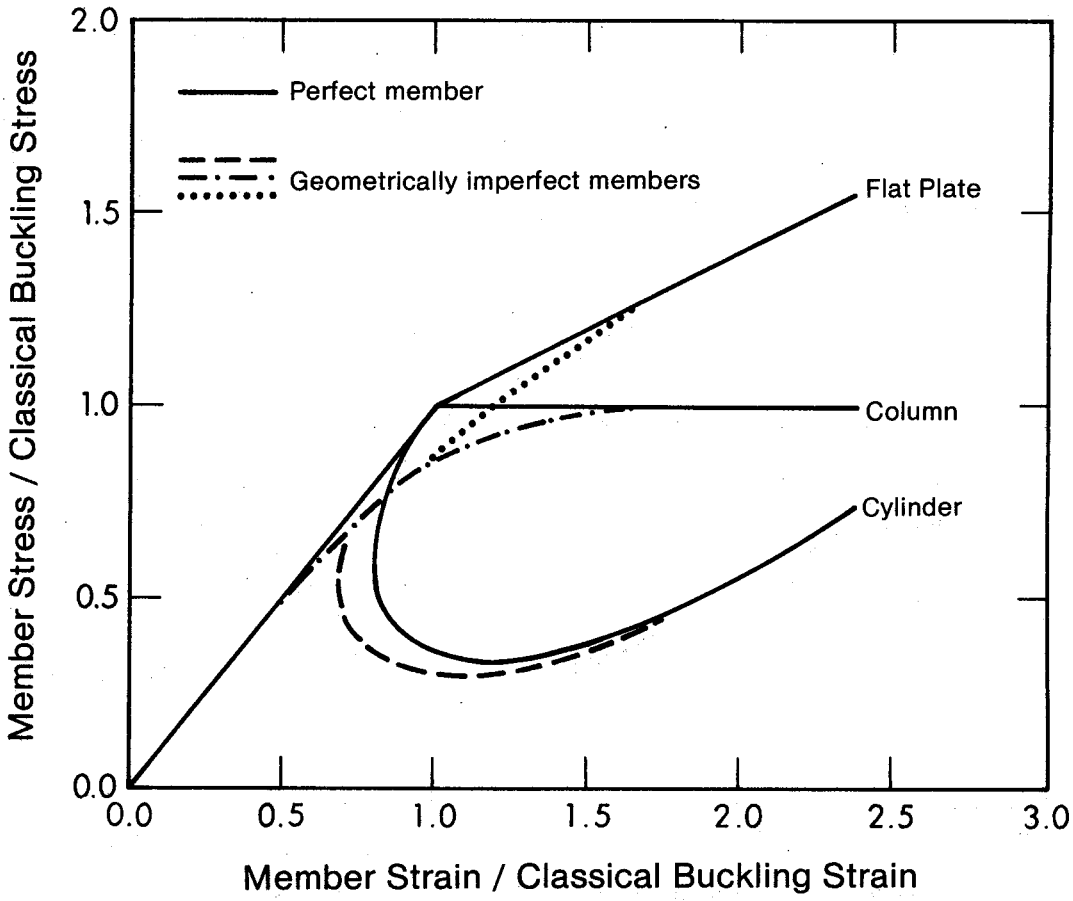

Figure 2.4 Postbuckling Behavior of Flat Plates, Columns, and Thin-Walled Clyinders

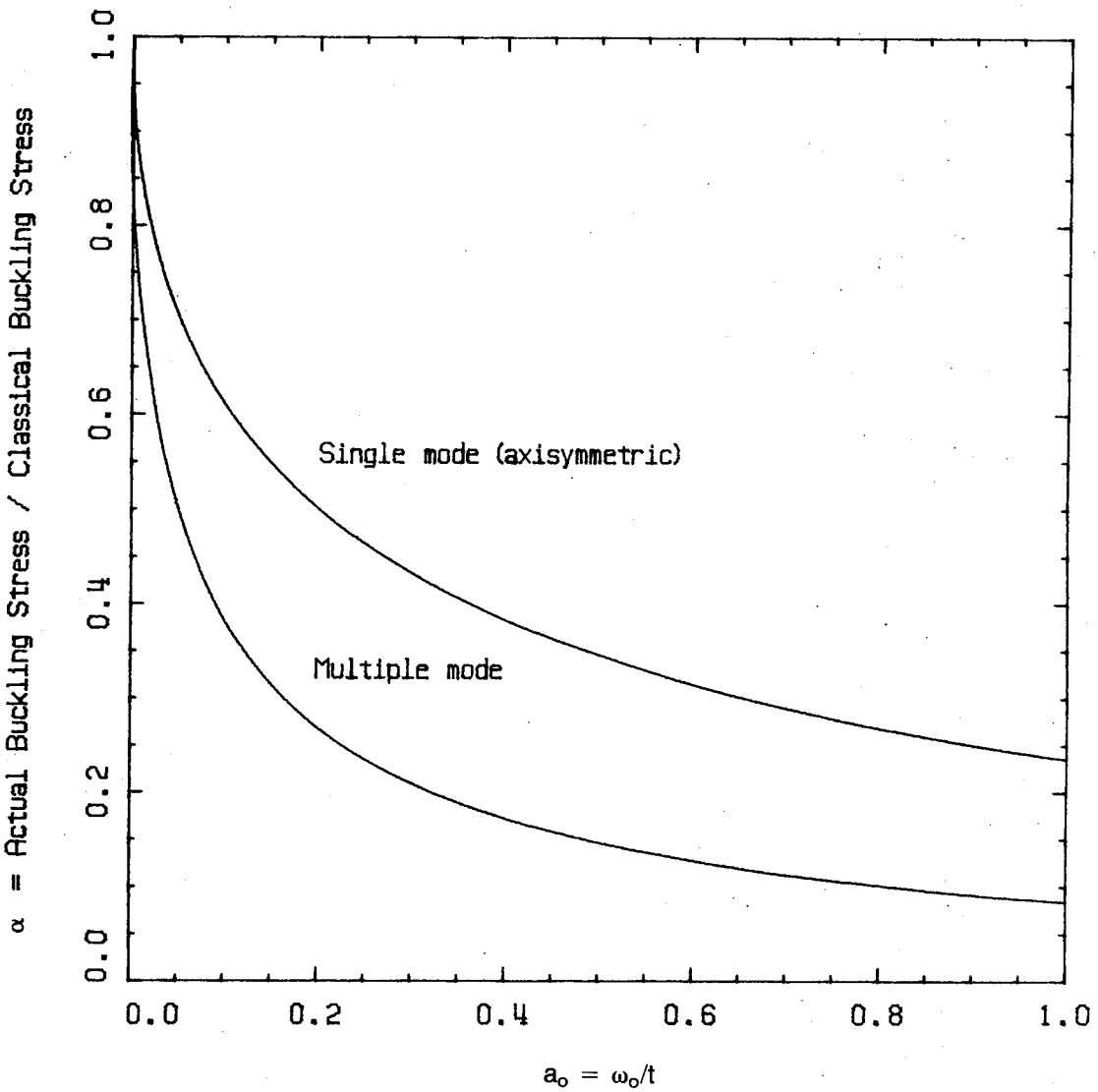

Figure 2.5 Effect of Single and Multiple Mode Imperfections on the Buckling Strength of Thin-Walled Cylinders

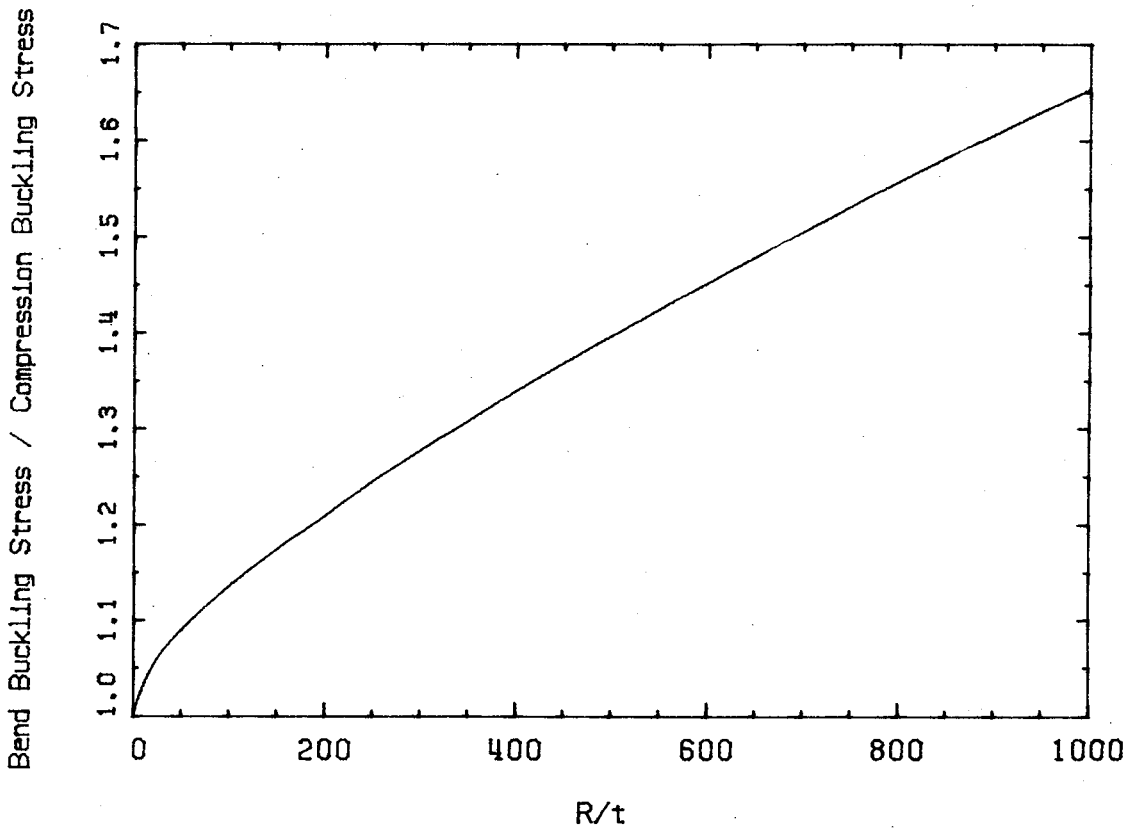

Figure 2.6 Increase in Elastic Flexural Buckling Strength of Aerospace Quality Specimens

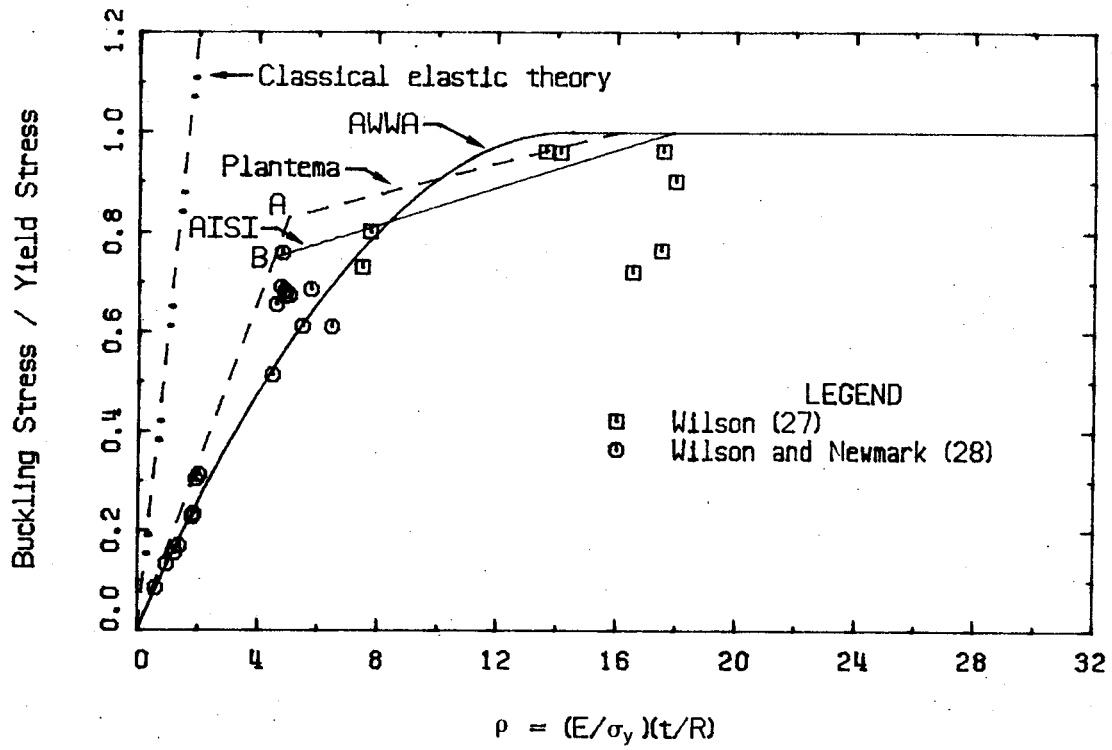

Figure 2.7 Local Buckling Ultimate Strength Curves

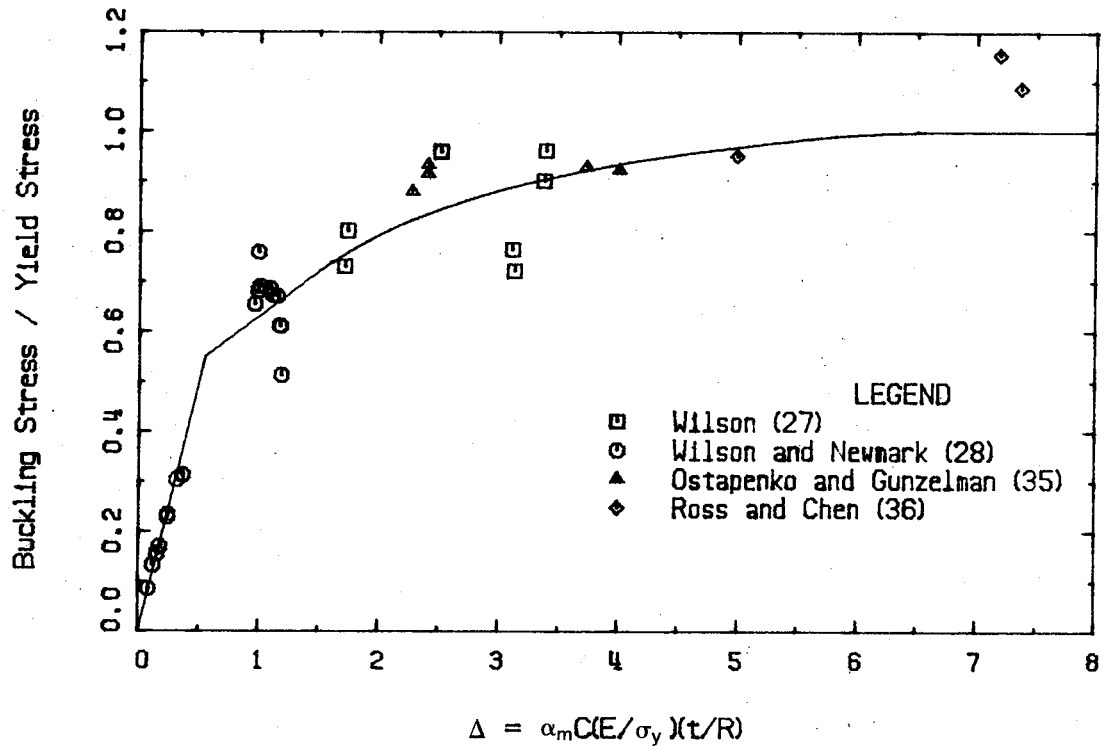

Figure 2.8 ASME Local Buckling Ultimate Strength Curve

3. EXPERIMENTAL STUDY OF FABRICATED CYLINDERS

3.1 Introduction

As indicated in Chapter 1, the purpose of the experimental program was to investigate the local buckling behavior of large diameter thin-walled fabricated cylinders loaded in either uniform axial compression or pure flexure. The cylinders tested herein cover a range of R/t from 149 to 222. In Western Canada, the most common use of cylinders of this geometry is for tubular conveyor galleries which range in diameter from 2400 mm to 4000 mm and are fabricated from steel plate ranging in thickness from 5 mm to 8 mm ($150 < R/t < 400$). In modelling these prototype structures the test specimens were made to approximately one-half of their full-scale diameter and plate thickness was adjusted accordingly.

While the main thrust of the experimental program was to obtain data for large diameter cylinders, the expense and time required to test cylinders of this type permitted the testing of only a few specimens. To augment these results, a preliminary series of tests on small-scale cylinders was carried out.

The preliminary series consisted of five small diameter cylinders loaded in uniform axial compression. In addition to supplementing the compression data base, these tests served to establish the most practical and effective method

of suppressing buckle formation at the ends of the specimens. This end effect results from stress concentrations caused by uneven bearing and the inducement of bending stresses in the cylinder wall. The bending stresses are the result of radial restraint imposed on the cylinder ends by the testing machine. Detrimental effects of this sort were reported by Wilson and Newmark (28).

A stiffening element was therefore introduced to resist the axisymmetric end buckling tendency and to force the buckle into the mid-height region. Cylinders were tested with various end stiffening configurations until the characteristic asymmetric buckle form was repeatedly observed in the central portion of the specimens.

Tests on large diameter cylinders involved four specimens, two loaded in pure compression and two loaded in pure flexure. The compression specimens were stiffened according to the guidelines established in the preliminary series. The compression series was significant in its own right since few tests on large diameter cylinders have been reported in the literature. It also served as a basis for evaluating the flexural tests. Because the flexural series involved the first such tests carried out on large diameter fabricated cylinders, it was important that they be closely linked to the more standard compression test.

3.2 Preliminary Considerations

As previously described, the buckling behavior of fabricated tubular members is considerably affected by the method of construction. In view of this, fabrication techniques employed were typical of those used in a structural fabrication shop. The large diameter specimens were fabricated by the Dominion Bridge Company at their Edmonton Plant using structural grade plate. The small diameter cylinders were fabricated at the University of Alberta. Because of the small thickness, sheet steel had to be used for these specimens rather than structural grade plate.

Flat plate coupons were cut from the material prior to rolling to permit the determination of the elastic modulus and the yield strength. The coupons were prepared in accordance with the appropriate ASTM Standard (39). Coupons were oriented so that material properties would be measured parallel to what would later be the longitudinal axis of the specimens. In all cases the yield stress measured was that corresponding to a zero strain rate (static yield).

3.3 Initial Geometric Imperfections

The theoretical and experimental work discussed in Chapter 2 indicates that initial geometric imperfections have a pronounced detrimental effect on the buckling strength of thin-walled cylinders. Consequently, the initial

geometry of the large diameter specimens was carefully measured to permit the determination of imperfection levels representative of those in fabricated cylinders.

3.3.1 Categorization of Imperfections

Three forms of shape deviation were considered. First, the overall shape deviation of the cross-section was established by measuring the cylinder out-of-roundness, O_r, defined as

$$O_r = D_{max} - D_{min} \tag{3.1}$$

where D_{max} and D_{min} are the maximum and minimum mutually perpendicular inside diameters of a particular cross-section. Second, the local bulges and depressions in the cylinder wall surface were measured with respect to longitudinal reference lines. The surface imperfections measured in this way were characterized by the deviation amplitude, ω_o', defined as the offset between points on the wall surface and a best-fit straight line through those points over a given gage length. Finally, the uniform axisymmetric depressions that occurred at the circumferential welds in the bending specimens due to weld shrinkage were measured for amplitude (ω_o'').

3.3.2 Apparatus and Measuring Procedure

The device used to measure the imperfections is shown in Fig. 3.1. It permits the measurement (at discrete points on the cylinder wall) of specimen radii with respect to an assumed longitudinal axis. In measuring the large diameter specimens, the vertical dial gage spacing and the arc length of the circumferential interval were set at 230 mm and 305 mm, respectively. The gage length of the dial gage rack was 1370 mm. As a result, 16 radii measurements were taken at each of seven elevations, a total of 112 radii measurements for each cylinder.

Despite the large number of measurements taken, only a sampling of the local imperfection amplitudes was obtained. A complete mapping of the imperfection profiles would have required substantially more readings and was considered beyond the scope of this report. None the less, by combining collinear radii and comparing the differences in major and minor diameters thus obtained, out-of-roundness measurements were obtained with certainty.

3.4 Cylinders Subjected to Uniform Axial Compression

3.4.1 Specimen Description

The small diameter specimens in the preliminary compression series were rolled from 0.9 mm thick steel sheet. Longitudinal seams were joined with full-penetration

groove welds made by the manual shielded metal arc process using AWS E410xx electrodes. The diameter and length of all specimens was approximately 380 mm. Exact dimensions are given in Table 3.1.

The first specimen (SC1) was tested without end stiffening elements to serve as a control. The second specimen (SC2) was tested with longitudinal stiffening fins pop-riveted at close intervals around each end. The final three specimens (SC3, SC4, and SC5) were tested with ring stiffeners at each end. Seventy-five mm wide strips of 0.9 mm sheet metal were rolled and riveted to each cylinder end to form collars. Rivet spacing was increased towards the centre of each cylinder in the hope of gradually reducing the overall stiffening effect.

Specimen C1 in the large diameter compression series was fabricated from 5 mm thick CSA G40.21 300W steel plate. Specimen C2 was fabricated from 10 gage (3.5 mm) ASTM A36 steel plate. The material was cold formed in rollers to the desired curvature and joined with full-penetration groove welded butt splices made by the automatic submerged arc process using AWS E480xx electrodes. The diameter and length of specimen C1 was approximately 1525 mm whereas specimen C2 was 1525 mm in diameter and 1830 mm long. Exact dimensions are given in Table 3.1.

Stiffening collars for both specimens were rolled from 305 mm wide strips of 6 mm steel plate. They were attached to the cylinder ends with 14 mm diameter A325 bolts in

specimen C1 and plug welds in specimen C2. Stiffener dimensions and bolt hole spacings were proportional to those of the small diameter specimens. The bolting configuration is shown in Fig. 4.3.

3.4.2 Test Set-Up and Instrumentation

All compression tests were performed in a 7000 kN Material Testing System (MTS) hydraulic testing machine.

The small diameter specimens (SC series) were seated directly on the hardened steel platens of the testing machine. The lower platen was fixed and the upper platen was suspended from a ball and socket connection. No attempt was made to attach the specimens to the platens and therefore the cylinders were simply supported along the reaction surfaces but effectively restrained against radial movement by friction under load.

The preliminary series of specimens were tested with four equally spaced, longitudinally oriented electrical resistance strain gages attached around each cylinder at mid-height. This permitted the direct measurement of longitudinal strain and subsequent evaluation of load uniformity.

To test the large diameter specimens, a load-spreading frame was built to transfer the load from the small upper loading platen to the perimeter of the test specimen (Fig. 3.2). The base of the tube was seated on a ring of steel plates directly on the load bed. Reaction surfaces

were simply supported. As in the preliminary series, restraint against radial movement could be anticipated because of friction.

To measure longitudinal strain and load uniformity, two circumferential bands of eight electrical resistance strain gages were attached to the outer surface of the tube. Each circumferential band was 450 mm from the specimen mid-height.

3.4.3 Testing Procedure

The first phase of each test was to align the specimen in the testing machine. The small diameter specimens, which fitted directly on the machined platens, were fabricated with sufficient care that load uniformity was always obtained by simply centering the specimen under the load head. The large diameter specimen C1, however, required extensive shimming. Alignment was considered adequate when measured longitudinal strain increments were within 10% up to a load of approximately 35% of the estimated failure load. Load uniformity for specimen C2 was obtained more simply by grouting between the specimen and the end fixtures with a high-strength Portland cement grout.

In the testing of all compression specimens, finite load increments were applied, decreasing in size as the expected failure loads were approached. Strain gage and piston stroke readings were taken after each load increment.

3.5 Cylinders Subjected to Pure Flexure

3.5.1 Specimen Description

The two large diameter bending specimens were each constructed from three subsections which were subsequently welded together. All welds, both circumferential and longitudinal, were full-penetration groove welded butt splices. The automatic submerged arc process was employed using AWS E480xx electrodes. A completed tube consisted of a central test section 1525 mm in diameter and 1830 mm long, and two stiffer end sections each 1525 mm in diameter and 915 mm long. For specimen B1, the central section was fabricated from 5 mm thick CSA G40.21 300W steel plate with end sections of similar material 8 mm thick. Specimen B2 had a central section fabricated from 10 gage (3.5 mm) ASTM A36 steel plate and end sections 6 mm thick. Exact dimensions are listed in Table 3.1.

The end sections were fabricated from thicker material in order to provide a transition in cylinder wall stiffness from the ends of the test specimen towards the center. As with the stiffening collars used on the compression specimens, it was hoped that the stiffer end sections would restrict buckle formation to the thinner central section of the tube thus avoiding possible end effects.

3.5.2 Test Set-Up and Instrumentation

The test set-up used for the bending tests is shown in Fig. 3.3. External loads were applied to a composite test beam consisting of two relatively rigid end frames and a central tubular test member (Fig. 3.4). With the beam supported at each end and subjected to two-point loading at the frame-to-tube transitions, the central tubular member was contained within a region of pure bending.

In joining the tubular member to the end frames, 25 mm thick steel plates were first welded to each end of the tube. These plates were then bolted to connecting fixtures, consisting of a grillage of wide-flange and channel sections, which were in turn bolted to the inner end of each frame.

The load and reaction points were all simply supported on steel rockers. One end of the system was free to translate horizontally so as not to induce axial restraint. Lateral support for the system was provided by bracing the end frames.

An Amsler loading system was used to apply the concentrated forces. The system consists of two hydraulic jacks acting in parallel from a common pump. Each jack has a static load capacity of 1000 kN. This provided a maximum moment capacity for the test set-up of 4420 kN·m.

As shown in Fig. 3.5, electrical resistance strain gages were attached in circumferential bands of 16 to the outer surface of the central test section. The strain gages

were oriented to measure longitudinal strain. Rotation meters were attached at the neutral axis of the tube to permit indirect measurement of the curvature during loading (Specimen B1 only). Transducers were placed inside the central test section to measure flattening of the cross-section and dial gages were positioned at the level of the neutral axis to measure vertical deflection at various locations.

3.5.3 Testing Procedure

Alignment of the specimens was carried out by placing shims between the end frames and the tube end-plates. These were required to minimize the strains that were locked in upon bolting-up. Alignment was considered adequate when variations in locked in longitudinal stress were measured to be less than 10% of the estimated buckling stress.

In testing the specimens, the system was subjected to finite load increments which were decreased in size as the expected failure load was approached. Strain gage and transducer readings were taken after each load increment. Rotation meter and dial gage readings were taken at greater intervals.

Table 3.1 Geometry of Test Specimens

Series	Specimen	Material	Radius[1] mm	Length mm	Thickness mm	R/t	L/R	Remarks
Preliminary Series	SC1	Sheet	190.5	381.0	0.89	214.3	2.00	No collars (control specimen)
	SC2	"	190.5	381.0	0.89	214.3	2.00	Long. stiffeners (riveted)
	SC3	"	190.5	381.0	0.89	214.3	2.00	Collars at ends (riveted)
	SC4	"	186.0	381.0	0.86	215.6	2.05	Collars at ends (riveted)
	SC5	"	186.0	381.0	0.86	215.6	2.05	Collars at ends (riveted)
Compression	C1	300W	764.5	1524.0	5.13	149.0	1.99	Collars at ends (bolted)
	C2	A36	761.7	1828.8	3.43	222.2	2.40	Collars at ends (plug welded)
Bending	B1	300W	764.5	1828.8	5.13	149.0	1.99	Thickened tubular sections
	(ends)	"	(766.1)	(914.4)	(7.94)	(96.5)	(0.99)	at each end
	B2	A36	761.7	1828.8	3.43	222.2	2.00	Thickened tubular sections
	(ends)	"	(763.3)	(914.4)	(6.50)	(117.4)	(1.00)	at each end

1 Radius of middle surface

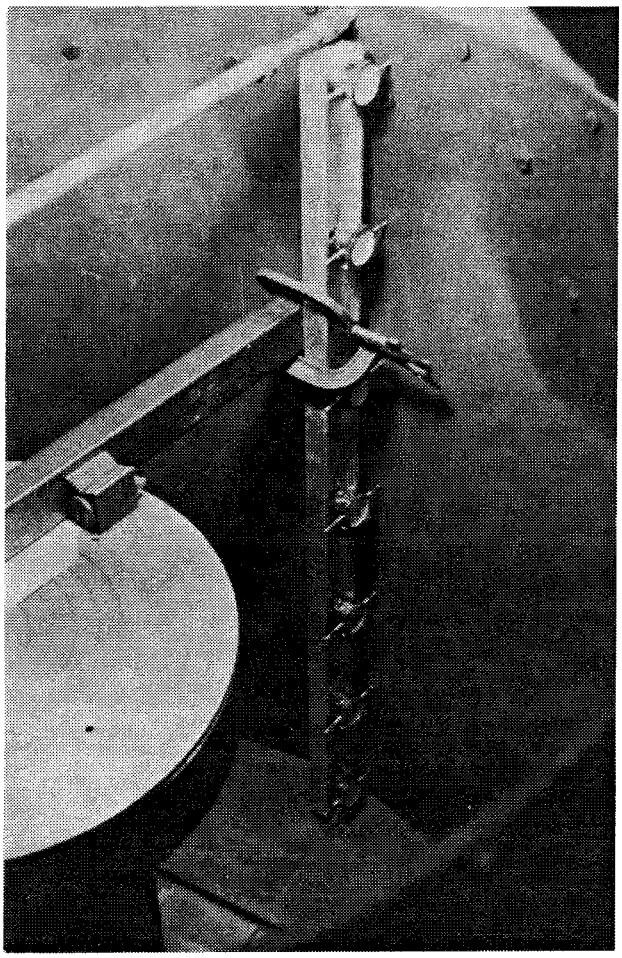

Figure 3.1 Imperfection Measuring Apparatus

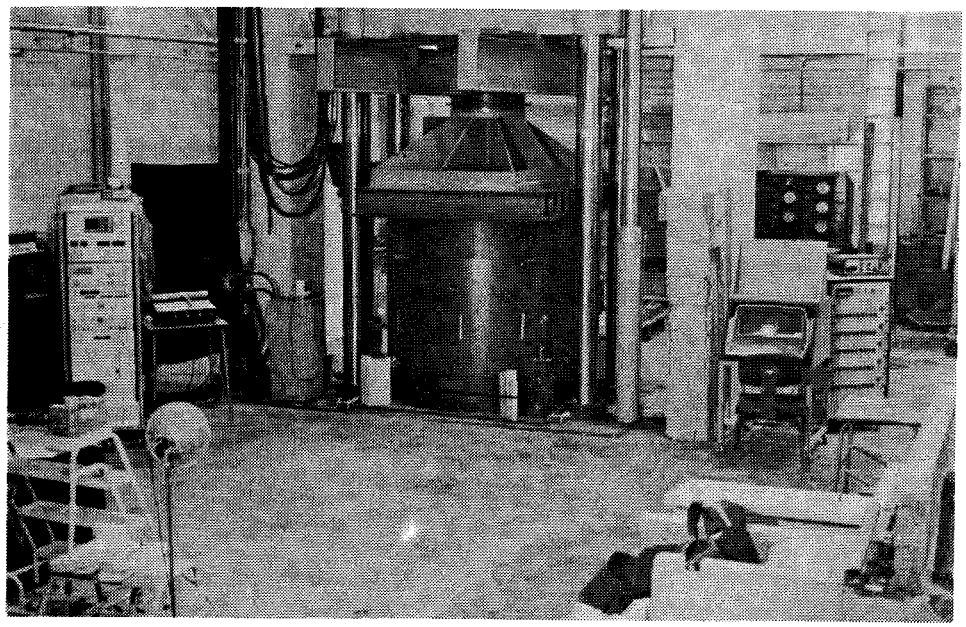

Figure 3.2 Test Set-Up for Large Diameter Compression Specimens

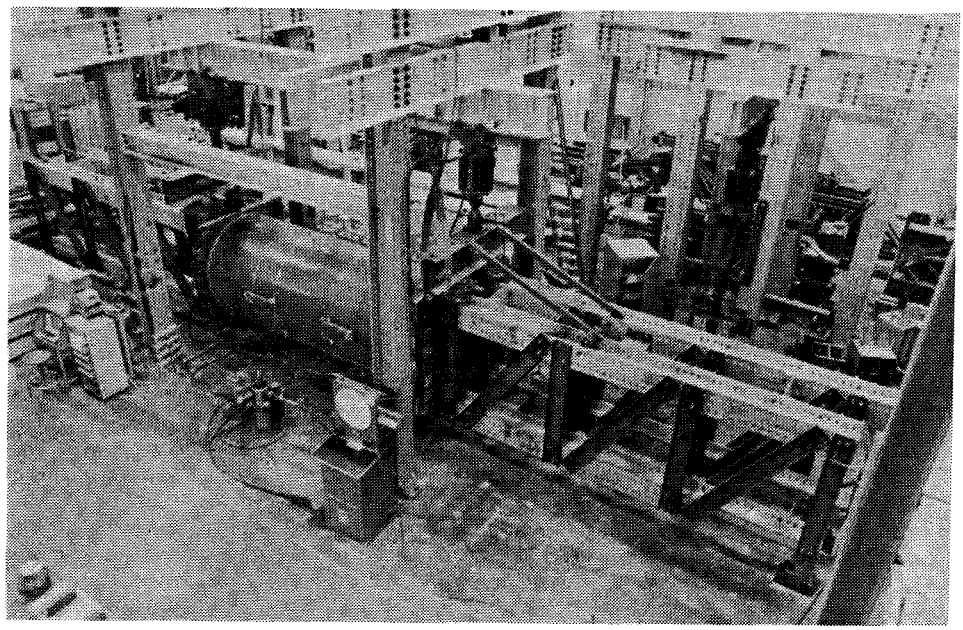

Figure 3.3 Test Set-Up for Bending Specimens

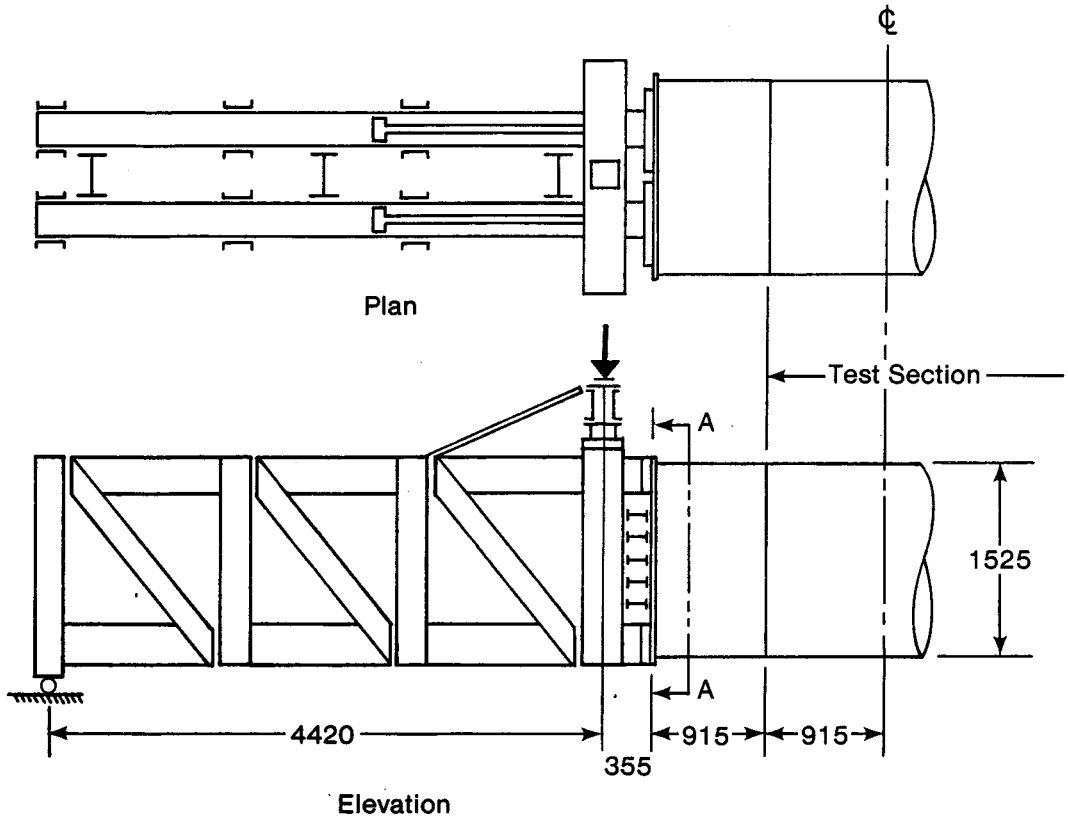

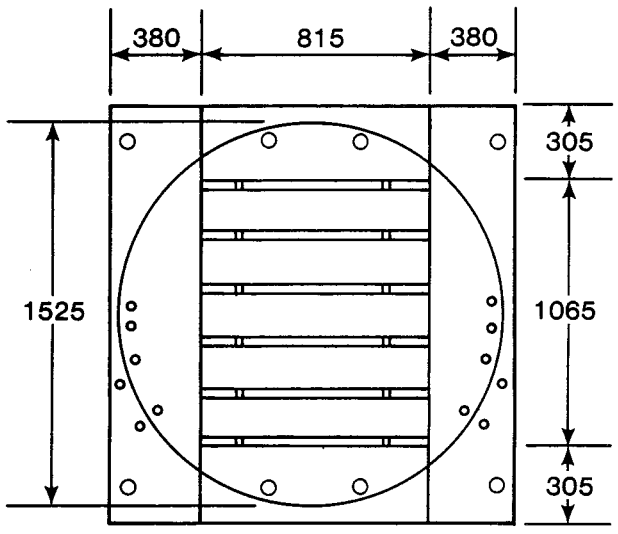

Figure 3.4 Composite Test Beam Used in Bending Tests

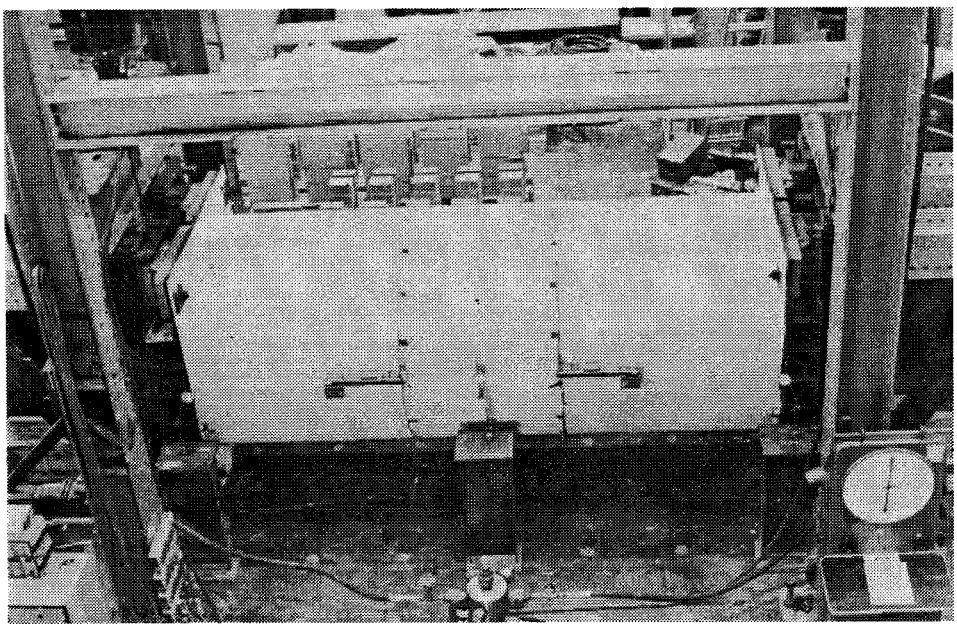

Figure 3.5 Instrumentation for Bending Specimens

4. TEST RESULTS

In this chapter, the results of the experimental program outlined in Chapter 3 are presented.

4.1 Material Properties

Table 4.1 lists the values of the elastic modulus and the static yield point as determined from tensile tests on coupons taken from the material used in the test specimens. In each case three coupon tests were performed and the average value is reported.

All coupons exhibited sharp-yielding behavior characteristic of unworked mild steels. No proportional limit was observed.

4.2 Imperfections in Large Diameter Specimens

The results of imperfection measurements for both the bending and compression specimens are summarized in Table 4.2.

The maximum value of the out-of-roundness, as calculated by Eq. 3.1, is reported for each specimen. For the compression specimens the maximum values were found to occur in sections closest to the ends. Out-of-roundness of the bending specimens was fairly uniform over the length of the test sections. It was also observed for both compression and bending specimens that the maximum and minimum diameters were more or less perpendicular to one another, giving the

specimens an oval or elliptical shape.

In calculating the deviation amplitudes, ω_o', no distinction was made between inward and outward deviations. Average and maximum values of the absolute values of the deviations are tabulated. Also given is the root mean square (rms) of the deviations, defined as

$$\text{rms} = \left[\frac{\Sigma(\omega_0)^2}{s} \right]^{1/2} \qquad (4.1)$$

where s is the number of readings. This value is considered because Tennyson *et al.* (40) have found it to be the best single measure of imperfection amplitude for cases where the amplitude is a statistically random variable.

Finally, the average, rms, and maximum values are given for the depression amplitudes, ω_o'', measured at the circumferential groove welds in the bending specimens.

4.3 Compression Test Results

4.3.1 General Observations

All specimens failed as a result of local buckling at a longitudinal compressive stress level below the static yield point of the material.

In the preliminary series, the unstiffened control specimen, SC1, failed when an axisymmetric ring-shaped buckle formed at the bottom of the cylinder. Likewise, the

fin-stiffened specimen, SC2, failed at the base in an asymmetric mode. The end failure of both specimens is indicative of the previously discussed detrimental effects of edge restraint. Test results for cylinders SC1 and SC2 are therefore not included in this report.

The ring-stiffened specimens in the preliminary series (SC3, SC4, and SC5) formed asymmetric depressed diamond-shaped buckles in the unstiffened portion of the tube. Specimen SC3 buckled at mid-height (Fig. 4.1a) whereas the buckles in specimens SC4 and SC5 formed closer to the collars (Fig. 4.1b).

Both specimens in the large diameter series (C1 and C2) collapsed into buckled forms similar to those observed in the small diameter specimens SC4 and SC5 (Fig. 4.2). Asymmetric buckles formed above the lower stiffening collar in specimen C1 and below the upper collar in specimen C2. The buckled shapes of the large diameter specimens are shown in Figs. 4.3 and 4.4.

4.3.2 Behavior During Loading

As shown by the plots of axial load versus end shortening in Figs. 4.5 and 4.6, all specimens exhibited similar behavior prior to failure. During the initial loading stages, nonlinearity was observed due to seating of the specimens. Following this, linear elastic behavior was observed up to a proportional limit, as substantiated by cyclic preliminary loading. Beyond this point there was a

gradual reduction in axial stiffness. Failure resulted from sudden buckle formation and immediate subsequent collapse.

The white-washing applied to specimens C1 and C2 to give a visual indication of large surface strain indicated that no local yielding was observable prior to failure.

Specimens SC3, SC4, and SC5 failed at loads of 173 kN, 134 kN, and 127 kN respectively. Large diameter specimen C1 failed at 6917 kN and specimen C2 at a load of 4306 kN.

The average compressive stress at the proportional limit and at failure are given for each specimen in Table 4.3. In all cases this average stress was determined by dividing the external load by the cross-sectional area of the specimen.

Flexibility in the compression end fixtures used in testing the large diameter specimens resulted in longitudinal stress variations in excess of 10% of the average values. Maximum deviations from the average values are also presented in Table 4.3.

4.4 Bending Test Results

4.4.1 General Observations

Specimens B1 and B2 failed by local buckling at loads less than those required to produce the theoretical moment at first yield. In both specimens, depressed diamond-shaped buckles formed in the extreme compression region of the central test section adjacent to the circumferential groove welds that joined the test section to the thicker end sections. The asymmetric buckling commenced with a single depression centered on the extreme compression fiber at about 150 mm from the circumferential weld. Buckling spread symmetrically about the top fiber, and in its final form, three distinct lobes were observed covering about 3/7 of the circumference in both specimens. The buckled form of specimen B1 is shown in Figs. 4.7 and 4.8.

Specimen B2 was retested after longitudinal stiffeners were welded to the tube in the region of the buckle. The size and distribution of the stiffeners, shown in Fig. 4.9, was chosen so as to replace approximately 90% of the cross-sectional area of the cylinder in the buckled region. They were of sufficient length to extend beyond the points where the longitudinal buckle waves terminated.

The failure mode of the stiffened version was identical to that of the unstiffened version. Depressed diamond-shaped buckles formed near the center of the test section about 75 mm from the ends of the stiffening elements.

4.4.2 Behavior During Loading

The behavior of bending specimen B1 is shown in Fig. 4.10 where a plot of moment versus curvature of the central test section is presented. The curvatures shown are derived from strain gage readings, rotation meter readings, and deflection dial gage readings. Also shown is the curvature expected if linear beam theory is assumed.

The curvature calculated from the longitudinal strain gage readings was the average curvature determined from the difference in strain between the extreme compression and tension regions. The strains used to calculate the curvature were measured at 12 gage locations; three in compression and three in tension, at each of two cross-sections.

The curvature based on rotation meter readings was calculated from the change in slope between the meters attached to each end of the central test section at the neutral axis. The curvature shown is the average value.

Curvature calculated from the dial gage readings was based on the averaged deflection of the assumed neutral axis, at the center of the test section, relative to the ends of the thickened sections. The curvature so calculated was corrected for the effects of circumferential straining of a tubular member loaded in pure flexure which causes points originally at the assumed neutral axis to shift downward along the arc of the tube. In correcting for this Poisson effect, the cylinder wall was assumed to be in a state of plane stress and Poisson's ratio was taken as 0.3.

The assumption of plane stress implies that the welded connections at the ends of the tube do not impose restraint against circumferential straining at the mid-section. This assumption was supported by circumferential strain measurements which indicated strains slightly in excess of those expected for a tangentially unrestrained tube. The correction amounted to a 6% reduction in calculated curvature. For comparison purposes, a curve showing uncorrected curvature is also given in Fig. 4.10.

It can be seen from Fig. 4.10 that the specimen behavior was practically linear up to a moment of 1770 kN·m. The slight nonlinear behavior at lower loads was the result of flexibility in the tension region of the tube-to-frame connecting fixtures rather than inelastic behavior of the test section. The nonlinear strain distribution, induced in the tubular member by this flexibility, spread through the thickened end sections into the central test section under increasing load. Deflection gage readings and rotation meter readings reflected the effects of this disturbance. The effect on strain gage readings, though not readily apparent in Fig. 4.10, is shown clearly in Fig. 4.11 which gives the average strain distribution in the test section at various moment increments.

When the external moment exceeded 1770 kN·m, substantial nonlinear behavior was indicated by the rotation meters and deflection gages. Shortly thereafter, local yielding (as indicated by flaking of the white-wash) was

observed near the circumferential groove welds between the central and end sections. This occurred on the test section side in the extreme compression zone and was first noted at a moment of 1860 kN·m. The local yielding spread towards the neutral axis at both ends of the test section as load was increased.

Flattening of the cross-section, as determined by the change in vertical diameter at three cross-sections, reached a maximum of 1.52 mm prior to failure. This amount of ovaling (0.20% of the initial radius) would have a negligible effect on both the local radius of curvature and the moment of inertia.

The buckling failure was sudden, and was followed by a substantial drop in the load carrying capacity of the member. The moment at failure was 2143 kN·m. This corresponds to an extreme fiber stress of 228 MPa based on linear beam theory. However, the nonlinear strain distribution caused by flexibility of the connecting fixtures resulted in tensile strains less than those expected by beam theory. To maintain equilibrium, the neutral axis of the specimen shifted upward and the compressive stress in the extreme fiber region increased. The maximum measured strain corresponded to a compressive stress of 262 MPa. This is about 15% in excess of that predicted by beam theory. Adding the measured initial stresses resulting from welding, bolting, and specimen dead load (Fig. 4.11), which in the extreme compression region

averaged 34 MPa, the total compressive stress at failure was 296 MPa. The maximum effective compression stresses corresponding to the proportional limit and the failure moment of specimen B1 are listed in Table 4.3.

Because of equipment difficulties which arose during the testing of specimen B2, only the moment at failure was recorded. In the absence of strain gage readings it was impossible to determine the maximum compression stress directly. However, the linearity of behavior exhibited during trial loadings of this specimen, and the minimal amount of end fixture plate seperation observed during the testing of specimen B1 at lower loads, supports the hypothesis that strain distribution was in accordance with elastic beam theory. The assumption of linear behavior throughout the loading history is also supported by the observation that no local yielding occurred prior to failure. (In specimen B1, the onset of local yielding in the area of the circumferential welds was synonymous with nonlinear behavior.)

The failure moment of 1028 kN·m corresponds to a theoretical extreme fiber stress of 164 MPa using beam theory. Together with the initial stresses resulting from welding, bolting, and dead load, the total extreme fiber compression stress was 190 MPa.

The retesting of specimen B2, after the attachment of longitudinal stiffeners, was carried out in the same manner as for specimen B1. The stiffening of a discrete portion of

the specimen altered the behavior of the cylinder to a certain extent. Consequently, the loading behavior of the stiffened specimen is not presented since it is not considered representative of the phenomenon under investigation. Despite this, certain results are significant and are presented for qualitative discussion.

Ovaling of the cross-section was measured and found to be negligible, amounting to 2.54 mm, or 0.33% of the initial radius, prior to failure.

The stiffened specimen sustained a slightly larger moment than the unstiffened specimen. It failed at a moment of 1140 kN·m with a corresponding maximum compressive stress of 179 MPa. In an overall sense the stiffeners did not significantly alter the strain distribution during loading: the maximum compressive stress at failure was only 1.5% less than that predicted by beam theory.

Plastic deformations that occurred during the buckling of the unstiffened tube left residual tensile stresses in the compression region of the stiffened version. These tensile stresses were of sufficient magnitude to almost exactly cancel the compressive stresses initially induced by welding and dead load. Subsequently, the net compressive stress at failure was 180 MPa, slightly less than the failure stress for the unstiffened tube.

As with the unstiffened version, there was no indication of local yielding along the circumferential welds in the compressive zone, reinforcing the assumption that

linear behavior was in effect until failure. The proportional limit and the failure stress for specimen B2, both in the unstiffened form, B2a, and stiffened form, B2b, are given in Table 4.3.

Table 4.1 Material Properties

Series	Specimen	Material	E MPa	σ_{ys} MPa
Preliminary Compression	SC1,SC2,SC3	Sheet	195 800	239
	SC4,SC5	Sheet	205 100	203
Compression	C1	300W	202 000	376
	C2	A36	204 000	306
Bending	B1	300W	202 000	376
	B2	A36	204 000	306

Table 4.2 Initial Geometric Imperfections in Large Diameter Specimens[1]

Specimen	Out-of-Roundness (O_r) mm	Wall Deviation Amplitude (ω_o') mm				Weld Depression Amplitude (ω_o'') mm			
	Maximum	Average	rms	Maximum	Expected[2]	Average	rms	Maximum	Expected[2]
C1	5.01	0.270 (0.0525)	0.374 (0.0728)	1.744 (0.340)	0.274 (0.0535)	———	———	———	———
C2	15.23	0.148 (0.0430)	0.226 (0.0659)	1.140 (0.332)	0.293 (0.0855)	———	———	———	———
B1	4.66	0.364 (0.0708)	0.440 (0.0856)	1.524 (0.297)	0.274 (0.0535)	1.016 (0.198)	1.082 (0.211)	1.524 (0.297)	1.098 (0.214)
B2	12.69	0.190 (0.0556)	0.310 (0.0904)	2.184 (0.637)	0.293 (0.0855)	1.938 (0.565)	2.058 (0.600)	3.176 (0.926)	1.176 (0.343)

1 numbers in parenthesis are nondimensional amplitudes $(a_o) = \omega_o/t$

2 "Expected" values are based on Koiter's imperfection theory (see Section 5.1)

Table 4.3 Proportional Limits and Failure Stresses for Compression and Bending Specimens

Series	Specimen	σ_p MPa	σ_p/σ_{ys}	σ_u MPa	σ_u/σ_{ys}	Buckle Form	No. of Lobes -circumferential- Actual	Projected[1]
Preliminary Compression	SC3	146	0.611	163	0.682	Asymmetric	7	10
	SC4	123	0.606	133	0.655	Asymmetric	7	9
	SC5	116	0.571	125	0.616	Asymmetric	4	8
Compression	C1	229 (+45,-21)[2]	0.609	279 (+56,-27)[2]	0.742	Asymmetric	5	8
	C2	177 (+8,-17)[2]	0.578	263 (+11,-32)[2]	0.859	Asymmetric	3	7
Bending	B1	231	0.614	296	0.787	Asymmetric	3	7
	B2a	———	———	190	0.621	Asymmetric	3	7
	B2b	———	———	180	0.585	Asymmetric	3	7

1 Number of buckle lobes had waves formed around entire circumference of specimen

2 Numbers in parenthesis are maximum deviations in longitudinal stress as measured by strain gages

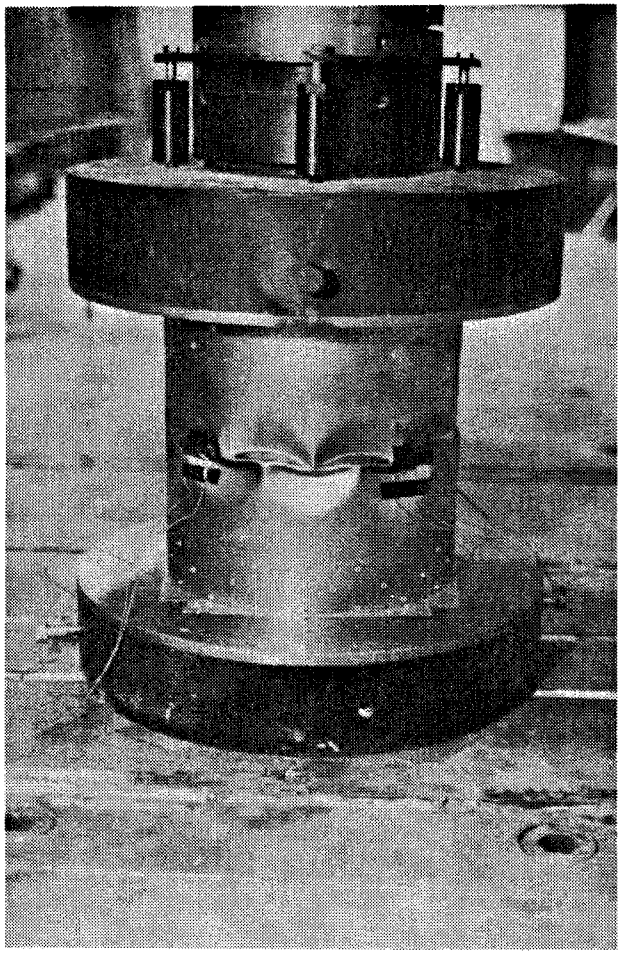

(a) Specimen SC3

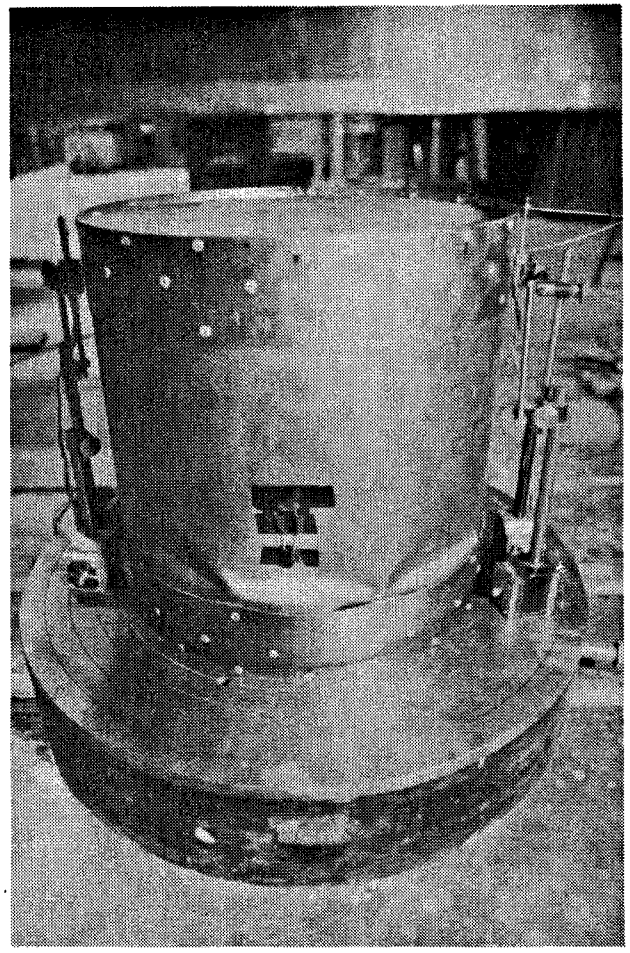

(b) Specimen SC4

Figure 4.1 Buckled Shape of Compression Specimens in Preliminary Series

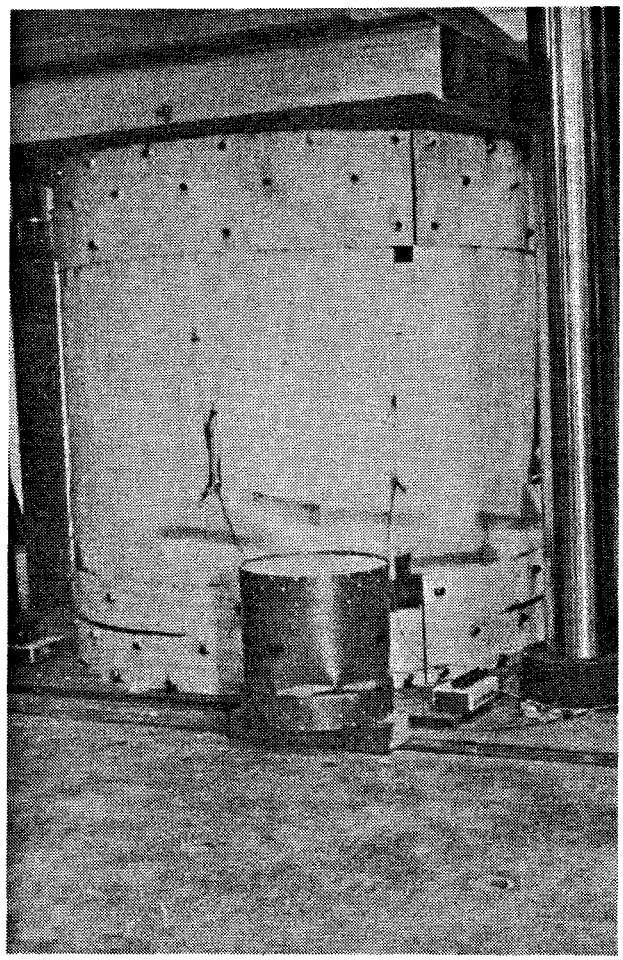

Figure 4.2 Comparison of Buckled Shapes Between Large and Small Diameter Compression Specimens

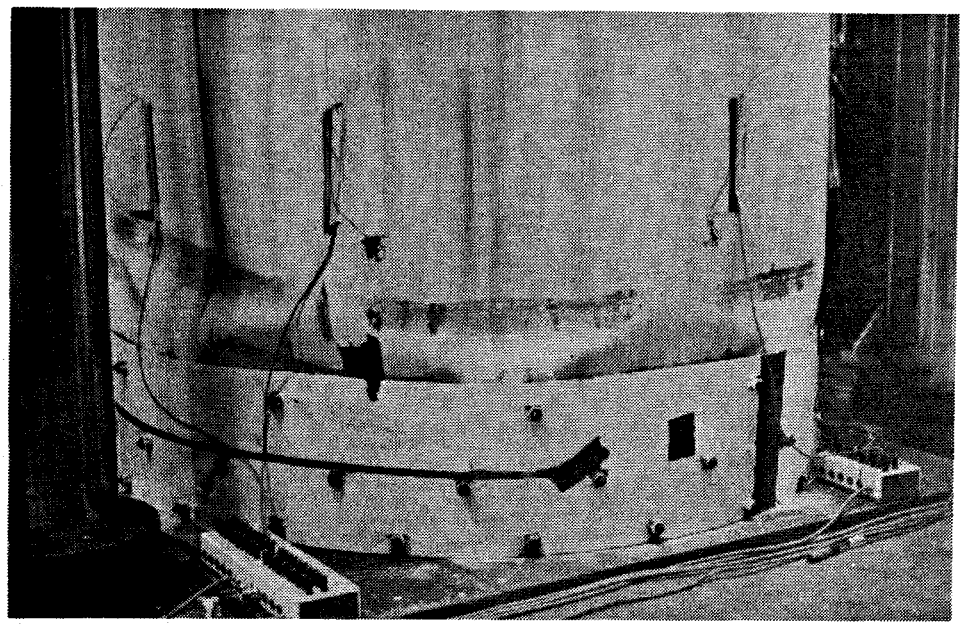

Figure 4.3 Buckled Shape of Compression Specimen C1

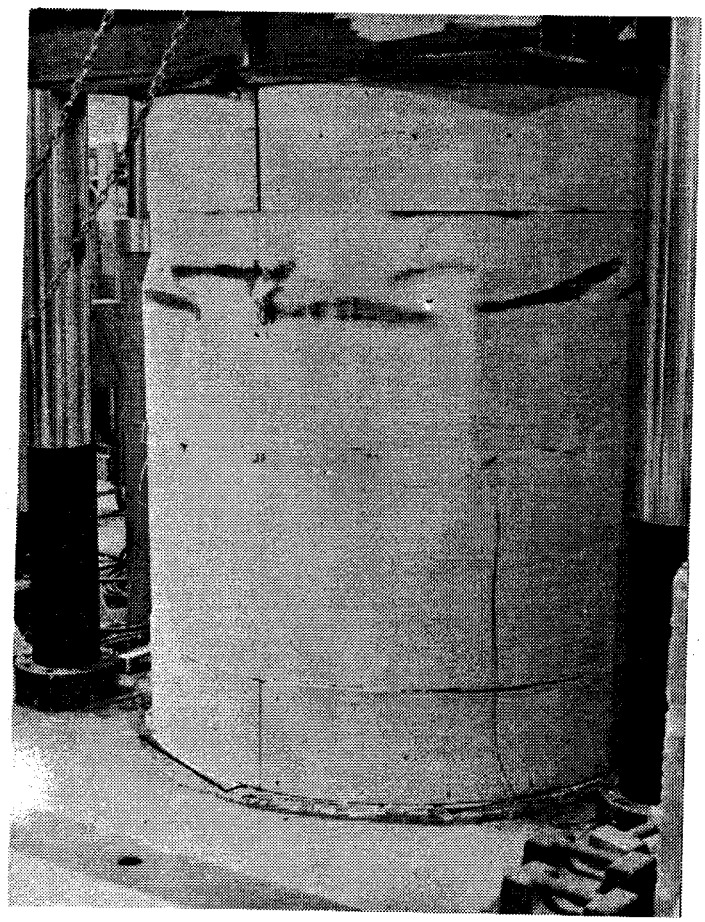

Figure 4.4 Buckled Shape of Compression Specimen C2

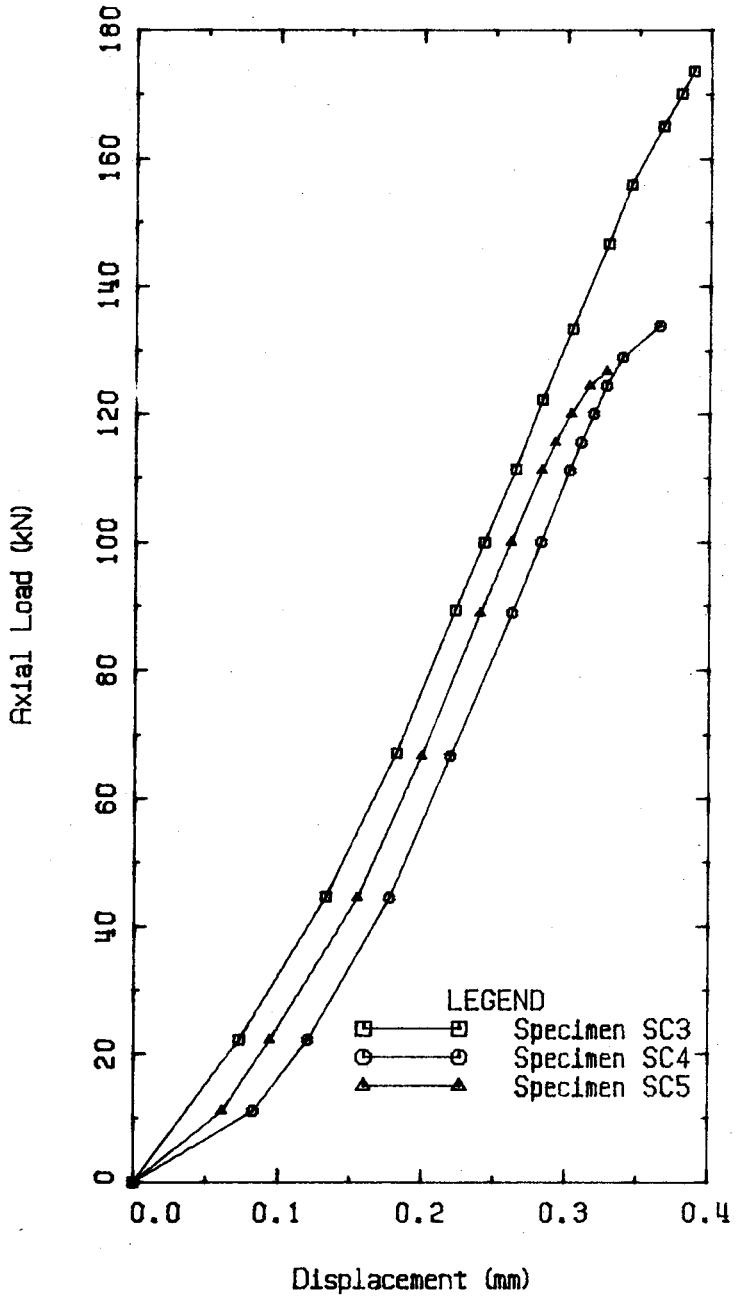

Figure 4.5 Load-Displacement Behavior of Preliminary Compression Specimens

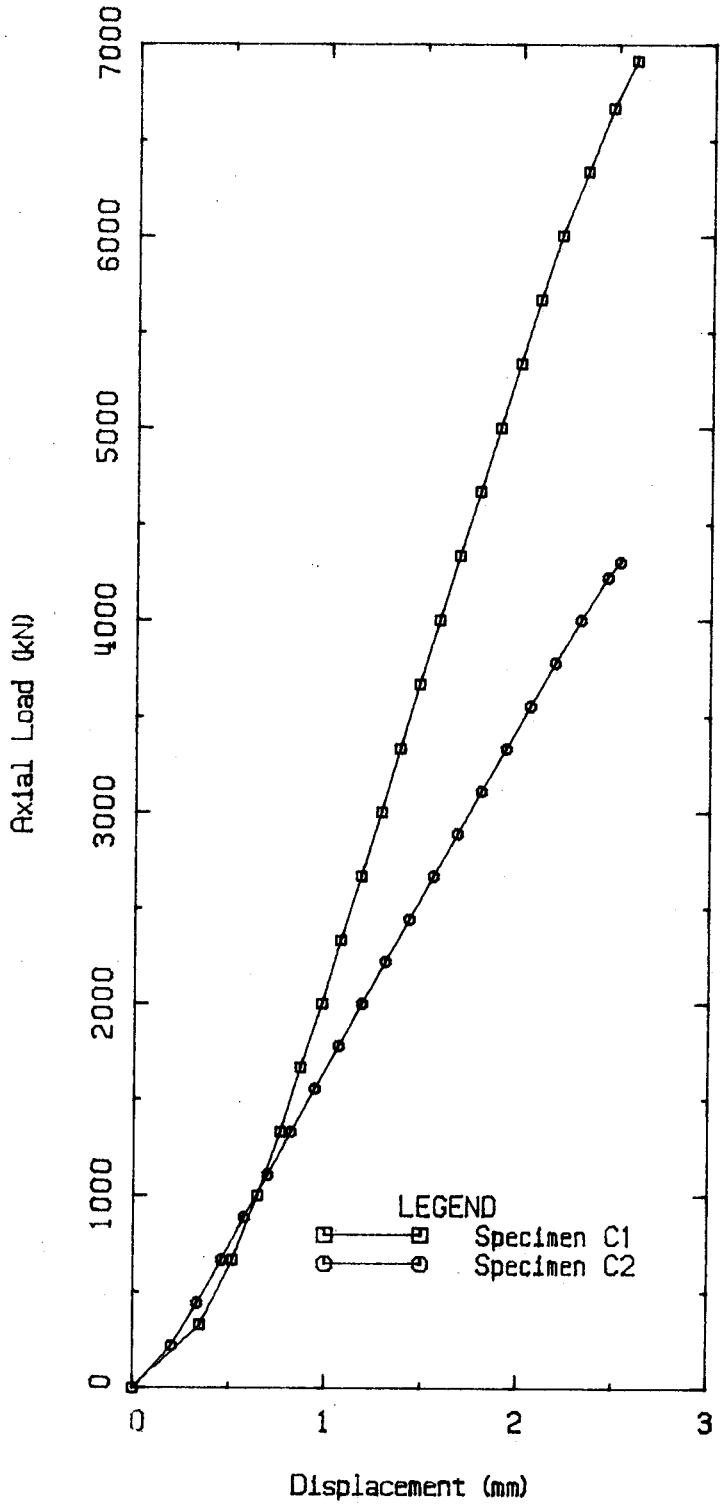

Figure 4.6 Load-Displacement Behavior of Large Diameter Compression Specimens

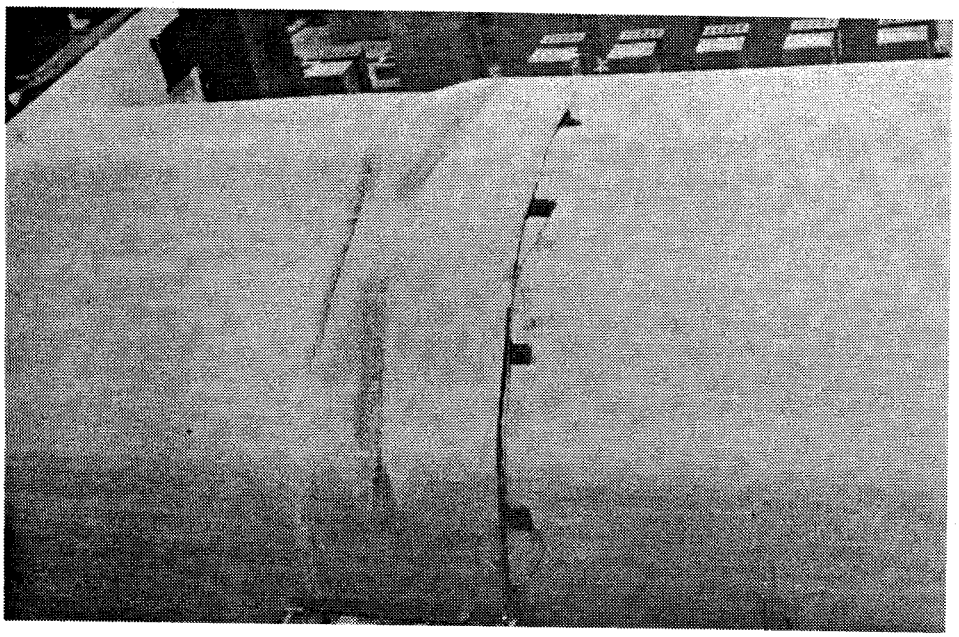

Figure 4.7 Buckled Shape of Bending Specimen B1

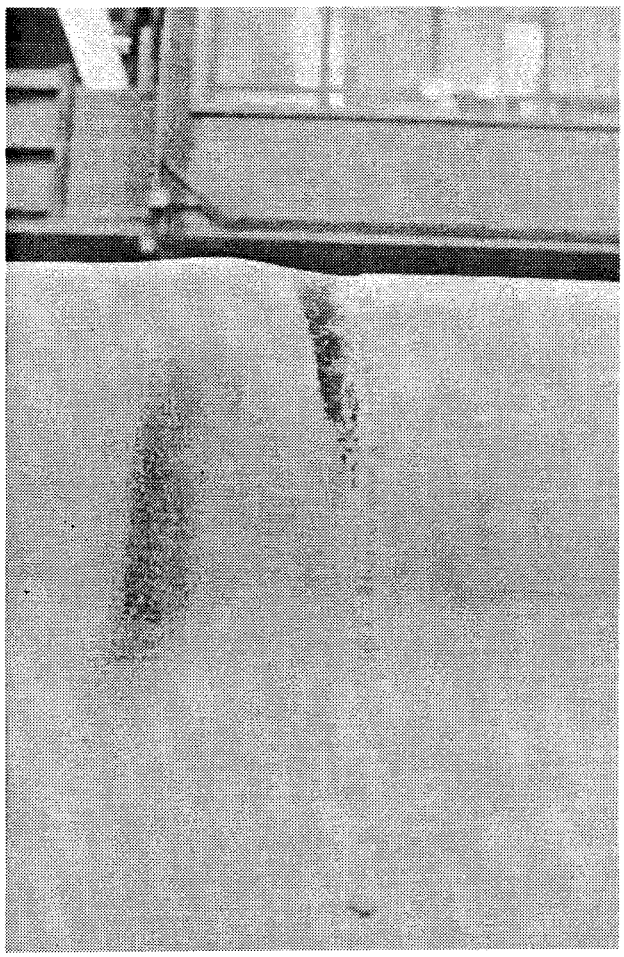

Figure 4.8 Proximity of Buckles to Circumferential Weld in Bending Specimen B1

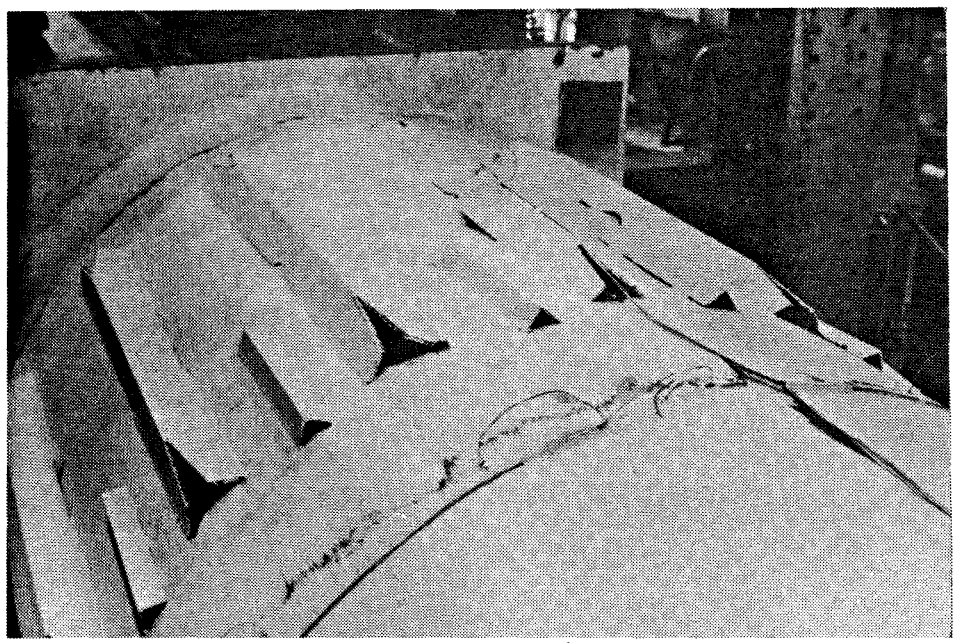

Figure 4.9 Stiffened Configuration of Bending Specimen B2

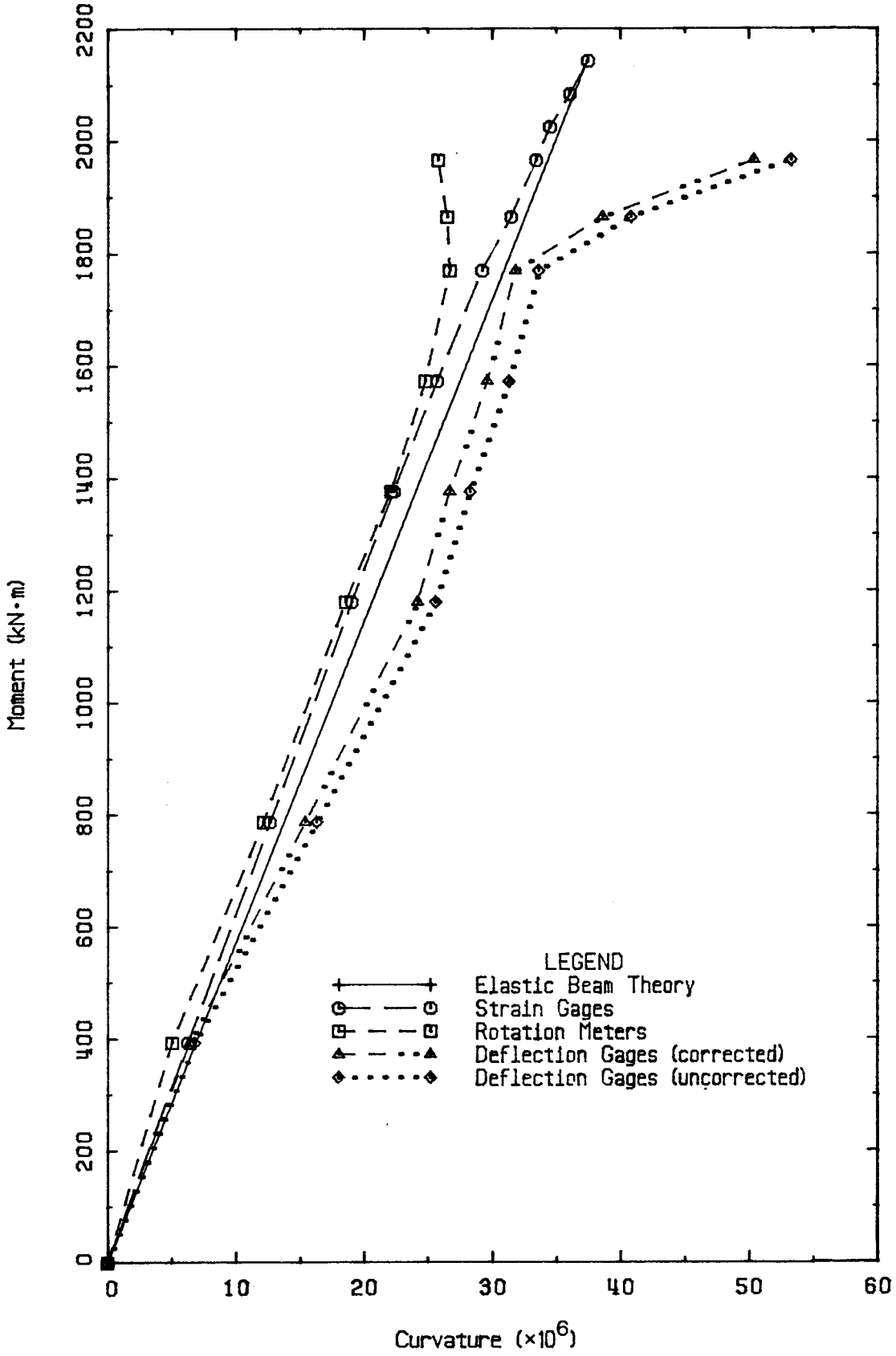

Figure 4.10 Moment-Curvature Behavior of Bending Specimen B1

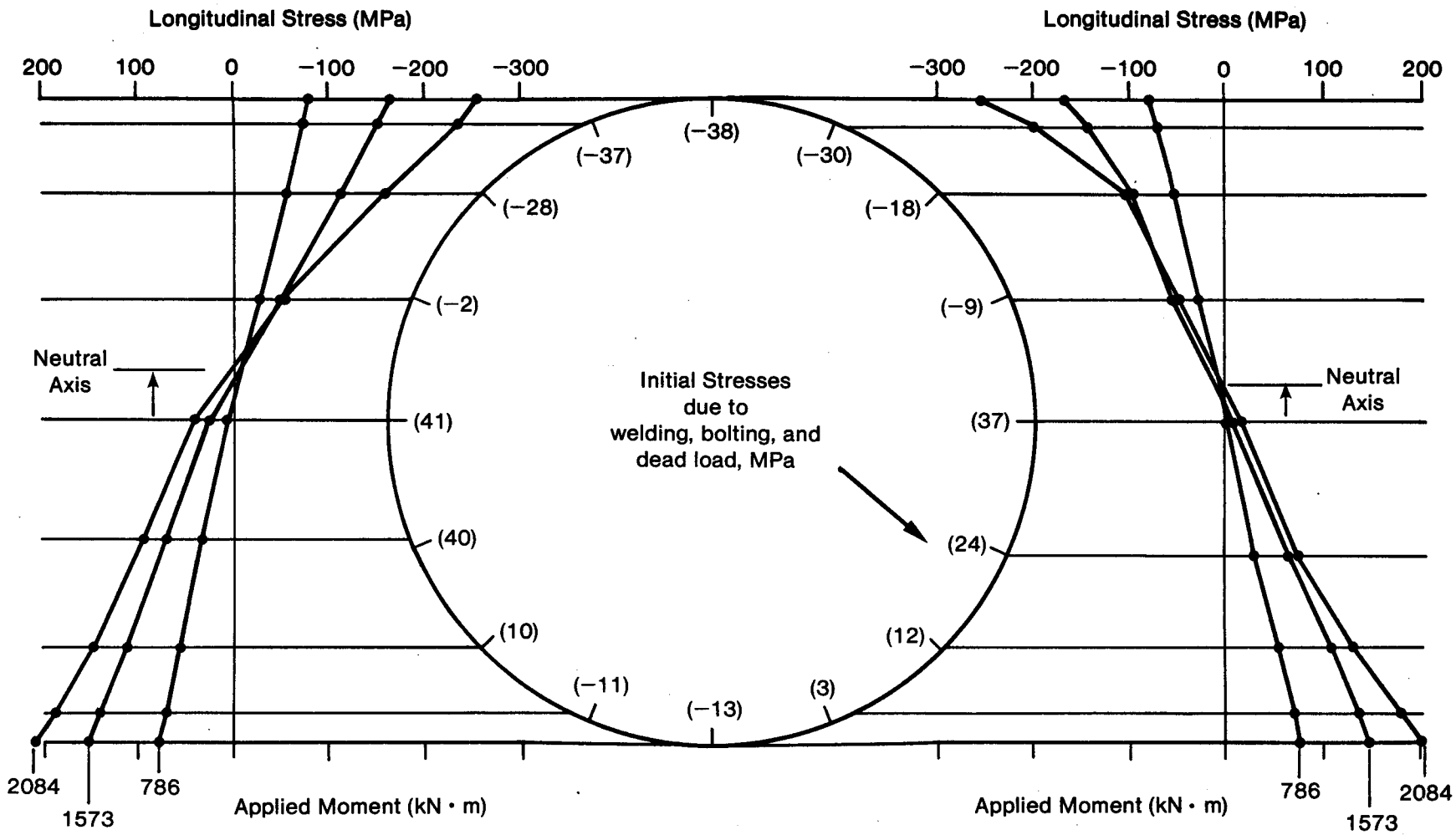

Figure 4.11 Longitudinal Stress Distribution in Bending Specimen B1

5. DISCUSSION OF TEST RESULTS

5.1 Introduction

In this chapter the test results are discussed within the context of the theoretical and empirical work set out in Chapter 2. The measured levels of geometric imperfection are compared with the limitations given by design specifications, and an attempt is made to ascertain the effect of various shape deviations on the local buckling strength. The compression test results are discussed and compared with the test results obtained by others, and the relative merits of the available design equations are examined. An alternate local buckling strength curve is presented which is shown to give a good fit to the test data for fabricated cylinders loaded in axial compression. The bending test results are discussed and compared with the compression test results to see if an increased flexural buckling capacity is indicated.

5.2 Initial Imperfections

The measured maximum imperfection levels are given in Table 5.1 along with the corresponding fabrication tolerances provided by various design specifications. It is seen that only some of the specifications give limitations that relate directly to the type of shape deviations measured herein. This can be attributed to the fact that the

effects of deviations from an assumed perfect cylindrical shape are not easily assessed from either a theoretical or an experimental point of view. The limitations, where given, are therefore based primarily on engineering judgement.

Considering first the specimen out-of-roundness, it was found that all specimens except compression specimen C2 were within the allowable range (Table 5.1). Specimen C2 exceeded the American Petroleum Institute (API) tolerance for fabricated steel pipe (41) by 20%. However, the consequences of exceeding the out-of-roundness limitations are not severe. Unlike local wall imperfections, which are known to significantly affect the buckling capacity, out-of-roundness or ovaling simply alters the basic geometry of the cylinder. Specifically, the effect is to change both the local radius of curvature and the bending moment of inertia of the cross-section. If the amount of ovaling is small, as it is in this case, the effects can be ignored.

For example, if the deformed shape of specimen C2 is approximated by an ellipse, the maximum local R/t ratio is only about 1.5% larger than for a circular shape. Similarly, the moment of inertia for bending about the major axis is reduced by only 1.25%. Since this is the worst case, it is clear that the effects of specimen out-of-roundness are negligible.

Local wall imperfections were, in all cases, within the specified fabrication tolerences. Previous investigations have shown, however, that even small amplitude imperfections

have a significant effect on buckling strength. Using the semi-empirical equation developed by Miller for the ASME Code (Eq. 2.11b), the expected reduction in buckling stress caused by imperfections can be calculated in the form of representative capacity reduction factors. The factors so determined are considered appropriate to the cylinder imperfections measured herein because of the acceptable agreement between the actual buckling stress and the ASME predicted buckling stress (to be discussed in detail later, see Section 5.3.2.3). The capacity reduction factors obtained using Eq. 2.11b are $\alpha_m = 0.49$ for specimens C1 and B1, and $\alpha_m = 0.41$ for specimens C2 and B2. These values imply that a 51% to 59% reduction in buckling stress (below the classical value) can be attributed to local wall imperfections alone. This does not include the additional reduction in strength caused by inelastic material behavior.

Incorporating the calculated α_m values into the imperfection theory of Koiter using Fig. 2.5, imperfection amplitudes can be determined. These are tabulated in Table 4.2 as expected values. An assumption made to facilitate comparison was that the random local wall deviations, ω_o', can be thought of as multi-modal imperfection amplitudes, and the circumferential weld depression amplitudes, ω_o'', as single mode axisymmetric imperfection amplitudes. It should be noted that the expected amplitudes are determined from capacity reduction factors which are primarily intended to account for the

effect of random surface imperfections characterized by ω_o'. The expected values for the axisymmetric imperfections, ω_o'', are those that would produce an equivalent reduction in buckling strength.

Correlation is seen to be acceptable between the expected values and either the average or root mean square (rms) of the measured values. The maximum measured values were in all cases considerably larger than the expected values. This indicates that a representative critical imperfection amplitude is more closely approximated by an average value rather than an extreme value. Best agreement was obtained using the rms values which, by definition, are weighted slightly in favor of the larger values. In comparing amplitudes, however, it must be realized that the expected values are based on a lower bound approximation to the widely scattered test data, and Koiter's assumed imperfection mode shapes. This, together with the small number of specimens measured, makes precise agreement between measured and expected values unlikely.

In comparing measured imperfection levels between specimens, it is observed that the bending specimens exhibit a higher level of random multi-modal imperfection than the compression specimens, even though the corresponding compression specimens were rolled from the same piece of steel plate. Since the only difference in fabrication was the presence of circumferential welds in the bending specimens, it might be concluded that the effect of these

transverse welds extends beyond the immediate weld depression area. This in turn might imply that tests on cylinders fabricated from single curved plates, without transverse welds, are not necessarily representative of members fabricated from many cylindrical segments.

Considering only the bending specimens, and comparing the magnitudes of the random multi-modal and axisymmetric weld imperfection amplitudes, a further observation can be made. Whereas the multi-modal imperfections are dominant for specimen B1, the axisymmetric weld depression in the thinner specimen, B2, is the dominant imperfection. This follows from the fact that the measured depression amplitude in specimen B2 greatly exceeds the value required to produce a detrimental effect equivalent to that of the random multi-modal imperfections.

This observation leads to the hypothesis that circumferential groove welds on tubes with wall thicknesses approaching that of specimen B2 ($t = 3.4$ mm), result in excessive initial axisymmetric imperfection levels which are not representative of the levels typically encountered in thicker tubes. This rationale is implied in both the AWWA and ASME design specifications which restrict their applicability to cylinders with wall thicknesses not less than 6.35 mm. Their limiting wall thickness, however, seems overly conservative in view of the fact that specimen B1, with a wall thickness of 5.1 mm did not show signs of excessive transverse weld depression. Again, these

conclusions are limited by the small number of specimens upon which observations were made.

5.3 Behavior of Cylinders in Compression and Bending

5.3.1 General Considerations

In evaluating the results of the buckling strength tests performed in this study, and in comparing them with the existing test data, it is convenient to deal with the cylinder strength and geometry in nondimensional form. Proportional limits and buckling stresses are nondimensionalized using the yield point of the material; geometric variations are expressed using the buckling parameter $Et/\sigma_y R$ established by Plantema (30).

In order to compare results obtained by other investigators, it is necessary to establish a relationship between the dynamic yield point, σ_{yd}, and the static yield point, σ_{ys}, of the material. Some experimenters report static yield values while others give dynamic values measured at an unspecified strain rate.

On the basis of the empirical formulas developed by Rao *et al.* (42), and by Ostapenko and Gunzelman (35), and assuming a strain rate for dynamic yield measurements midway between the maximum and minimum rates specified by the ASTM (39), the following ratios were established:

$\frac{\sigma_{yd}}{\sigma_{ys}} = 1.09$ for low to intermediate strength carbon steels

$\frac{\sigma_{yd}}{\sigma_{ys}} = 1.05$ for quenched and tempered, high-strength steels.

5.3.2 Compression Tests

5.3.2.1 Proportional Limit

Table 4.3 shows that the proportional limit expressed as a fraction of the yield point is remarkably consistent within both the preliminary series and the large diameter series. The measured values differ by less than 5%. The average proportional limit for the preliminary compression series was 60% of the static yield point or 55% of the dynamic yield point. For the large diameter compression series, the average value was 59% of the static yield point or 54% of the dynamic yield point. These values are in good agreement with the proportional limits defined by the ASME and ECCS design specifications as 55% and 50% of the dynamic yield point. The proportional limit of 75% of the dynamic yield level, indicated by the AISI specification, seems unconservatively high.

5.3.2.2 Local Buckling Strength

As expected, all specimens in both the preliminary and large diameter series failed at a small fraction of the classical elastic buckling stress as calculated from Eq. 2.1. This has been the case with all similar tests performed to date. In comparing the results obtained herein

with those obtained by others, it is important to restrict consideration to tests on specimens in which local buckling alone produced failure. Tests on specimens significantly longer than Miller's limiting value for L/R (See Eq. 2.12), were therefore excluded to ensure that the reported buckling strengths were not reduced through interaction with overall column buckling. In addition, selected tests in which specimen damage occurred prior to testing, or in which compressive strain uniformity during loading was suspect, were ignored. To remove from consideration the effect of excessive transverse weld depressions (Section 5.1) circumferentially welded cylinders with wall thicknesses less than 6 mm were also excluded.

Test data obtained by others that meet the above requirements (27,28,35,43,44,45,46) are plotted in Fig. 5.1 together with the test results obtained in this study. For uniformity, the dynamic yield point was used to nondimensionalize the data since most of the previous studies reported dynamic values.

With reference to the preliminary series of compression tests, it is significant that the results obtained are contained within the established scatter band. Firstly, this group of tests, on specimens nominally 0.8 mm thick, serves to link the main body of data ($\rho > 2.0$) to the remaining data points ($\rho < 2.0$). The latter consists solely of tests on cylinders which were fabricated from 0.8 mm material in a manner similar to that reported herein. Until now, the

degree to which the small-scale compression specimens model the behavior of full-scale large diameter specimens was in question. The results obtained in the present study tend to indicate that the small-scale fabricated specimens do give a valid representation of full-scale behavior. This, therefore, gives added credibility to the test results for very thin-walled cylinders ($\rho < 2.0$). Secondly, the representative behavior of the preliminary series indicates that the stiffening collars, subsequently used in the large diameter series, did not significantly affect the local buckling strength.

Considering the large diameter compression cylinders, it is observed that specimen C1 buckled at a stress tending towards the upper bound of the scatter band, and that specimen C2 buckled at a stress considerably higher than might have been expected on the basis of the other test results. This above average strength might indicate that the welding residual stresses and/or the initial imperfection levels in cylinders C1 and C2 were less than is usually the case for fabricated cylinders. The measured proportional limits and imperfection amplitudes do not, however, support this conclusion. The high buckling stresses also indicate that the circumferential variation in axial strain (caused by end fixture flexibility and uneven bearing) did not have a pronounced detrimental effect on buckling strength.

The higher capacity of specimen C2 relative to specimen C1 is, to a limited extent, supported by the imperfection

measurements made on the two cylinders. Table 4.2 shows that the imperfection amplitudes measured in specimen C2 were slightly smaller than those in specimen C1. This suggests the probability of a slightly higher relative buckling strength for specimen C2.

The expected trend towards a reduced buckling capacity with increased R/t ratio is not supported by the limited number of tests performed in this study. This is not surprising in view of the relatively narrow range of R/t ratios considered and the wide scatter normally associated with the compressive buckling capacity of cylinders.

5.3.2.3 Evaluation of Existing Design Specifications

Figures 5.2 through 5.5 are presented to illustrate the relative capability of the design equations reviewed in Chapter 2 to predict the local buckling ultimate strength of uniformly compressed cylinders. In comparing measured and predicted buckling stresses, the dynamic yield point was used to nondimensionalize the data since the equations considered were formulated on that basis.

The AISI formula (Eq. 2.6) applies to a limited range of R/t ratios. Therefore, in Fig. 5.2 the behavior of cylinders with R/t ratios exceeding the AISI limit of $44800/\sigma_{yd}$ are evaluated using the Plantema formula (Eq. 2.5), on which the more conservative AISI approach is based. Considerable scatter is observed, with the AISI equation predicting both conservative and unconservative

results. The Plantema equation for elastic buckling is seen to be unconservative for very thin-walled cylinders; predicted buckling stresses are in excess of 30% higher than measured buckling stresses.

The AWWA formula (Eq. 2.7) is found to significantly underestimate the buckling strength of cylinders with $150 < R/t < 600$ (See Fig. 5.3). This is because the strength equation was weighted downwards in the intermediate R/t range to account for some low buckling stresses obtained in investigations by Wilson (27) and Wilson and Newmark (28). These uncharacteristically low values (not plotted in Figs. 5.2-5.5) were the result of excessive specimen length and excessive circumferential weld depressions in very thin-walled tubes.

The more recent ASME approach (Eqs. 2.10 and 2.11) is shown in Fig. 5.4 to give a good lower bound to the test data over the entire range of R/t ratios considered. In addition, the data points fall within a much narrower scatter band. This reduction in scatter is achieved partly by the incorporation of the improved nondimensional buckling parameter, Δ, which accounts directly for the effects of geometric imperfections and their variation in size with R/t. For cylinders with low R/t ratios, a further improvement in correlation is achieved by the strictly empirical equation 2.11c which limits the magnitude of the elastic buckling capacity reduction factor α_m according to

σ_{yd} .

The ECCS approach (Eqs. 2.13 and 2.14) also gives acceptable correlation. Fig. 5.5 shows that the results are more uniformly conservative than the formulas incorporating the Plantema buckling parameter (AISI and AWWA). Compared to the ASME formula, however, the scatter is greater. In addition, the ECCS formula is somewhat overly conservative for cylinders with large R/t ratios.

It is important to note that the tests reported by Wilson (27) and Chen and Ross (43) were on cylinders which exceeded the ECCS length limit of $L/R < 0.95(Rt)^{1/2}$ (Eq. 2.17). The fact that these data points plot above the values predicted by the ECCS formula indicates that the specified length limitation is too conservative. This observation supports the use of the length limitation $L/R < 0.47(E/\sigma_u)^{1/2}$ (Eq. 2.12) adopted herein which permits the consideration of somewhat longer cylinders.

It can be concluded that the ASME design approach gives the best approximation of the local buckling strength of axially loaded fabricated cylinders, subject to the stated restrictions on length and wall thickness. Pending further investigation, the buckling strength of cylindrical members built up from welded segments, in which the wall thickness is less than about 6 mm, is better approximated by the more conservative AWWA formula.

It should also be noted that none of the design equations discussed suitably describe the results obtained

for the high-strength steels (σ_{yd} = 650 MPa) tested by Marzullo and Ostapenko (46). The tests which define the principle scatter band involved steels with yield points between 170 MPa and 410 MPa. It is appropriate, therefore, to restrict the applicability of the preceeding design formulas to cylinders fabricated from steels with yield points within the above range.

5.3.2.4 Alternate Local Buckling Ultimate Strength Formula

The design equations that best predict the local buckling capacity of compressed cylinders, namely, the ASME and ECCS equations, are not in a form particularly suitable for design. Various factors must be calculated and checked against limiting values in order to determine the predicted buckling stress. An attempt to simplify the procedure is presented herein.

As with the ASME formula, a buckling parameter is chosen to nondimensionalize the data and a local buckling ultimate strength curve is fitted through the principal band of the data points. The proposed buckling parameter is

$$\gamma = \left(\frac{E}{\sigma_y}\right)^{1/2} \left(\frac{t}{R}\right)^{3/2} \qquad (5.1)$$

Equation 5.1 is based on the panel strip theory proposed by Edlund (47) in 1977 to predict the local buckling strength of compressed cylindrical members.

In the panel strip theory, Edlund considers the general case of an asymmetric imperfection represented by a local dimple in the wall of an otherwise perfect cylinder. He assumes that the local buckling strength of the cylinder corresponds to the collapse load of an equivalent cylindrical panel containing the flattened region. In determining the collapse load of this flattened panel strip, it is assumed that, for a sufficiently narrow panel, the behavior coincides with that of a rectangular plate of equal thickness having a width, b, equal to the arc length of the panel. This leads to the use of a modified form of the ultimate plate strength formula originally proposed by von Kármán (48);

$$\frac{\sigma_u}{\sigma_y} = \left(\frac{\sigma_{el}}{\sigma_y}\right)^{1/2} \tag{5.2}$$

in which σ_{el} is the classical elastic buckling stress of a plate element;

$$\sigma_{el} = \frac{k\pi^2 E}{12(1-\nu^2)}\left(\frac{t}{b}\right)^2$$

and k is a constant that depends on the panel length and boundry conditions.

In establishing an equivalent panel width Edlund assumes that the ratio of the panel strip width to the

cylinder radius is proportional to $(R/t)^{1/2}$, hence

$$b = qR\left(\frac{R}{t}\right)^{1/2} \tag{5.3}$$

where q is a constant which depends on the level of imperfection.

Substituting Eq. 5.3 into 5.2 gives

$$\frac{\sigma_u}{\sigma_y} = C_\gamma \left(\frac{E}{\sigma_y}\right)^{1/2}\left(\frac{t}{R}\right)^{3/2} \tag{5.4}$$

$$= C_\gamma \gamma$$

where

$$C_\gamma = \frac{\pi}{q}\left[\frac{k}{12\,(1-\nu^2)}\right]^{1/2}$$

Equation 5.4 indicates that for cylinders with similar boundry conditions and imperfection levels, the buckling stress, as a fraction of the yield point, varies linearly with the buckling parameter γ.

In restricting the applicability of this theory, Edlund considers the procedure valid for calculating buckling stresses less than 80% of the yield stress. Furthermore, the assumption of elastic-plastic material behavior does not permit the consideration of residual stress effects which might be important in welded cylinders.

Edlund compared predictions using the panel strip theory with the test results obtained by Weingarten *et al.* (24) on aerospace quality specimens. Agreement was

found to be excellent with both the test results and the predictions based on Eq. 5.4 showing similar trends in their dependence on R/t. This indicates that the assumed relationship between panel strip width and cylinder geometry is reasonable.

In applying Eq. 5.4 to the test results on fabricated cylinders, it was decided to first nondimensionalize the results using the static yield point in order to eliminate the variability in measured dynamic yield point as a source of scatter. Agreement between theory and the experimental results obtained by Wilson and Newmark (28) was found to be good for cylinders that failed at less than 40% of the static yield point as shown in Fig. 5.6. The equation of the least squares best-fit line through the data points is

$$\frac{\sigma_u}{\sigma_{ys}} = 119.3\,\gamma_s \qquad (5.5)$$

where

$$\gamma_s = \left(\frac{E}{\sigma_{ys}}\right)^{1/2}\left(\frac{t}{R}\right)^{3/2}$$

No data is available on cylinders that fail between 40% and 60% of the yield point. Above 60% of σ_{ys}, the measured buckling stress falls increasingly below the value predicted by Eq. 5.5. Whereas the theory is suggested by Edlund to be valid for buckling stresses up to 80% of the yield point, the indicated reduction in the range of applicability is thought to be influenced by welding residual stresses. As previously discussed, this nonhomogeneity was not accounted

for in the derivation.

As an alternative to a linear best-fit, a curve was fitted to the test results on cylinders fabricated from mild steel plate (150 MPa < σ_{ys} < 400 MPa) for which the slenderness parameter, γ_s, was less than 0.10. Tests on cylinders with γ_s > 0.10 were not considered because the results consistently indicate that the yield stress is reached before buckling occurs.

As shown in Fig. 5.7, the data are closely grouped around a straight line on a semi-log plot. The equation of the least squares best-fit line through all the points is

$$\frac{\sigma_u}{\sigma_{ys}} = 1.625 + 0.489 \log \gamma_s \qquad (5.6)$$

Application of this equation is, however, restricted to a reduced range of γ_s values. For cylinders with γ_s less than 0.0036, Eq. 5.5 is a better estimate of the buckling stress; for γ_s greater than 0.0527, the buckling stress is limited to the yield stress. The equations which therefore define the proposed local buckling ultimate strength formula are:

$$\frac{\sigma_u}{\sigma_{ys}} = 119.3\ \gamma_s \qquad \text{for } \gamma_s \leq 0.0036 \qquad (5.5)$$

$$\frac{\sigma_u}{\sigma_{ys}} = 1.625 + 0.489 \log \gamma_s \qquad \text{for } 0.0036 < \gamma_s < 0.0527 \qquad (5.6)$$

$$\frac{\sigma_u}{\sigma_{ys}} = 1.0 \qquad \text{for } \gamma_s \geq 0.0527 \qquad (5.7)$$

These equations are plotted in Fig. 5.8 together with the available test results on fabricated steel cylinders loaded in axial compression.

In deriving Eq. 5.6, data points outside the subsequent range of application (those for which $\gamma_s \leq 0.0036$, and $\gamma_s \leq 0.0527$) were included in the best-fit evaluation. This was done to provide a more realistically gradual transition between the three curves which make up the composite buckling curve shown in Fig. 5.8.

To evaluate the goodness of fit of the proposed buckling formula, and to permit comparison with other design equations, the measured buckling stresses are normalized with respect to the predicted stress and plotted as a function of R/t in Fig. 5.9. It is seen that despite the best-fit nature of the equations involved, the formula provides a reasonable lower bound to the test results. The degree of scatter is found to be slightly greater than that encountered using the ASME formula (Fig. 5.4), but less than that associated with the ECCS formula (Fig. 5.5).

Of significance is the fact that the results obtained by Marzullo and Ostapenko (46) on high-strength steel tubes are more closely predicted by the proposed formula than by any of the existing design formulas. This is primarily attributed to the incorporation of $(E/\sigma_{ys})^{1/2}$ instead of E/σ_{ys} in the nondimensional buckling parameter γ_s.

Multiplying through by σ_{ys} in Eq. 5.5 gives

$$\sigma_u = 119.3 (E\sigma_{ys})^{1/2} \left(\frac{t}{R}\right)^{3/2} \qquad (5.8)$$

Eq. 5.8 shows that the buckling capacity of the tube depends on the strength of the steel supporting the buckle, even in the so-called elastic buckling stress range below the proportional limit. This sort of behavior, first noted by von Karmán (48) in tests on thin plates, is indicated for cylindrical members in an experimental investigation by Sherman (49), and is supported by Allen (50).

5.3.3 Bending Tests

5.3.3.1 Proportional Limit

Figure 4.10 shows that the proportional limit in specimen B1 occurred at a moment of 1770 kN·m and a measured extreme fiber compressive stress equal to 61% of the static yield point or 56% of the dynamic value. This limit agrees identically with the proportional limit measured in both the preliminary and large diameter series of compression tests.

Beyond the assumed proportional limit, hinging mechanisms began to form in the region of the circumferential welds between the test section and the thickened end sections. This hinging action was the result of local yielding of the test section in the compression zone. For a given external moment above 1770 kN·m, the

central test section translated downwards until, through the progression of yielding, equilibrium was attained in the region of the hinges. This accounts for the sharp increase in the centre line deflection of the specimen as indicated by the deflection based curvature in Fig. 4.10. Localized behavior, resulting from this hinging action in the regions surrounding the rotation meter attachment points is believed to account for their apparent indication of a reduction in curvature under increasing moment (Fig. 4.10).

In the testing of the unstiffened version of specimen B2, neither a proportional limit nor the associated hinging mechanism were observed prior to failure. This elastic behavior can be attributed to the low failure moment; it corresponded to an extreme fiber compression stress of only 62% of the static yield point or 57% of the dynamic value.

5,3.3.2 Local Buckling Strength

The bending specimens failed at extreme fiber compressive stresses well below the classical elastic buckling stress as determined using Eq. 2.1. Failure was precipitated by the circumferential welds which were a major source of geometric imperfection and residual stress; both have been shown to have a pronounced detrimental effect. The maximum compressive stresses are plotted as a fraction of the dynamic yield point in Fig. 5.1.

The tendency towards a reduction in buckling capacity with increased R/t is supported by the tests with specimen B2 (R/t = 222) failing at a smaller proportion of the yield stress than specimen B1 (R/t = 149). Considering only specimen B2, the slightly reduced buckling capacity of the locally stiffened version, B2b, relative to the unstiffened version, B2a, is attributed to weld shrinkage which occurred during stiffener attachment. This weld shrinkage induced additional geometric imperfections and residual stresses in regions adjacent to the stiffeners where buckles subsequently formed.

The degree to which the measured buckling strengths constitute behavior representative of flexurally loaded fabricated cylinders is uncertain. The results of only two tests are reported in this study and, as yet, no other similar tests have been performed on cylinders that buckle at stress levels below the yield point. Consequently, the only comparison that can be made is with the results for axially compressed cylinders.

In comparing the measured buckling strengths of the corresponding bending and compression specimens tested in this study, no definite trend is indicated. Bending specimen B1 buckled at an extreme fiber compressive stress 6% above the buckling stress of compression specimen C1, whereas specimen B2 buckled at a stress 28% below that of specimen C2. This inconsistency is attributed primarily to the uncharacteristically high buckling stress of compression

specimen C2. Contributing to a lesser extent were the circumferential welds in the bending specimens which had a greater effect on the thinner-walled specimen, B2.

The circumferential welds, in conjunction with the small thicknesses of the bending specimens, create further problems in comparing the results obtained herein to the relatively large body of compression test results obtained by others. The bending specimens were less than 6 mm thick, whereas the majority of the compression specimens tested were greater than 6 mm thick, if welded circumferentially. The only similar compression specimens were susceptible to column buckling because of excessive length.

It follows from above that a valid comparison between bending and compression is not yet possible. It is, however, significant that, in Fig. 5.10, both of the bending test results are seen to plot above the best-fit curve for compression developed in this study. Recalling that welded cylinders less than about 6 mm thick are expected to have a reduced buckling strength, the indication is that the buckling stress is slightly higher in flexure than in compression. This supports the hypothesis that the strain gradient present in a flexurally loaded member permits a higher maximum compressive stress than would be the case for a uniformly compressed member (See Section 2.4.2). Whether the increase is significant, however, remains to be established.

In view of the limited number of bending tests performed, the only thing that can be said with certainty is that the flexural buckling capacity of weld-fabricated cylinders can be approximated on the basis of the available test results for axially compressed cylinders. While an increased capacity in flexure is perhaps indicated, more testing is required to establish the amount by which the buckling stress is increased.

5.3.3.3 Comparison with Design Formulas

The flexural buckling stress for specimen B1 and the unstiffened version of specimen B2 are compared with the predicted buckling stresses in Table 5.2.

Considering only the ultimate strength formulas for compression, best agreement between the measured and predicted values is obtained using either the ASME approach (Eqs. 2.10 and 2.11) or the proposed approach (Eqs. 5.5, 5.6, and 5.7). Both formulas predict almost identical buckling strengths in the range of R/t which pertains to the two cylinders tested.

The ECCS approach (Eqs. 2.13 and 2.14) permits an increase in buckling strength for flexurally loaded members. This flexural buckling formula is shown to correlate as well with the test results as do the ASME and proposed formulas for compression. The ECCS formula for flexural buckling, however, is not recommended. The increased flexural capacity, which is assumed to be a function of R/t on the

basis of elastic buckling tests (24), has yet to be substantiated by flexural tests on fabricated mild steel cylinders over a sufficiently wide range of R/t.

Table 5.1 Comparison Between Maximum Measured and Allowable Imperfection Levels

Specimen	Out-of-Roundness (O_r) mm				Local Deviation Amplitude (ω_o) mm		
	Measured	AWWA	API	ASME	Measured ω_o' / ω_o''	AWWA	ECCS
C1	5.01	30.48	12.70	15.24	1.744 / ———	5.13	5.00
C2	15.23	30.48	12.70	15.24	1.140 / ———	3.43	4.08
B1	4.66	30.48	12.70	15.24	1.524 / 1.676	5.13	5.00
B2	12.69	30.48	12.70	15.24	2.184 / 3.176	3.43	4.08

Specification Fabrication Tolerences —

Out-of-Roundness: $O_r \leq 0.02\ Do^{1/2}$.....AWWA(31)

$O_r \leq 0.01\ Do^{1/3}$ | lesser
≤ 12.7 mm | value ...API(41)

$O_r \leq 0.01\ Do^{1/2}$.....ASME(34)

Deviation Amplitude: $\omega_o \leq t$.....AWWA(31)

$\omega_o \leq 2(Rt)^{1/2}/25$...ECCS(38)

1 Do = nominal specimen diameter

2 O_r calculated using maximum and minimum diameters (not necessarily mutually perpendicular)

3 O_r calculated using maximum and minimum mutually perpendicular diameters

Table 5.2 Comparison Between Measured and Predicted Buckling Stresses for Large Diameter Bending Specimens

Specification	Measured / Predicted	
	Specimen B1	Specimen B2
AISI-Plantema[1]	1.33	1.25
AWWA[1]	1.79	1.65
ASME[1]	1.15	0.99
ECCS[2]	1.14	1.03
Proposed[1]	1.13	1.05

1 Predicted buckling stress determined from a compressive buckling stress formula

2 Predicted buckling stress determined from a flexural buckling stress formula

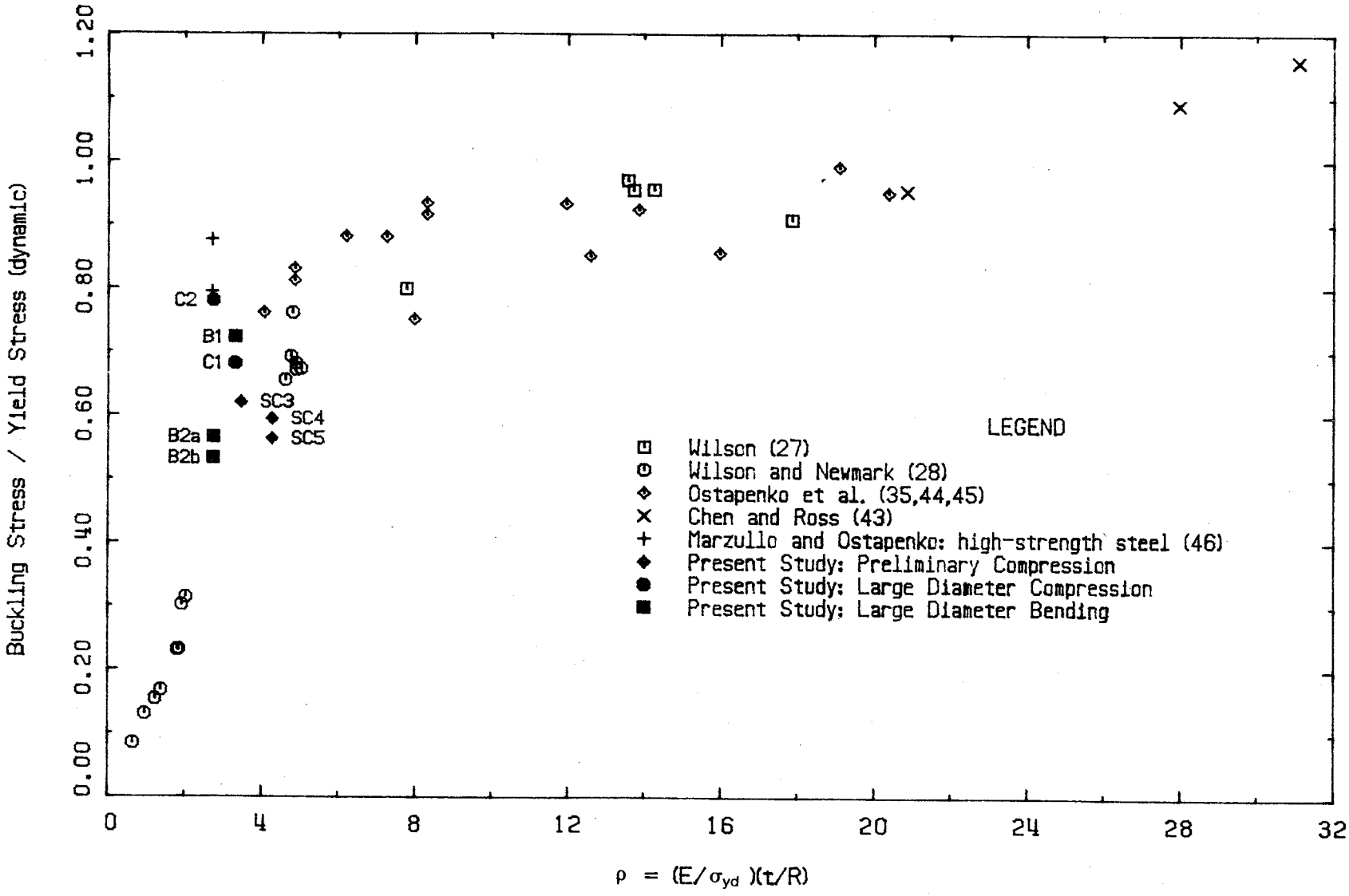

Figure 5.1 Local Buckling Ultimate Strength of Fabricated Steel Cylinders

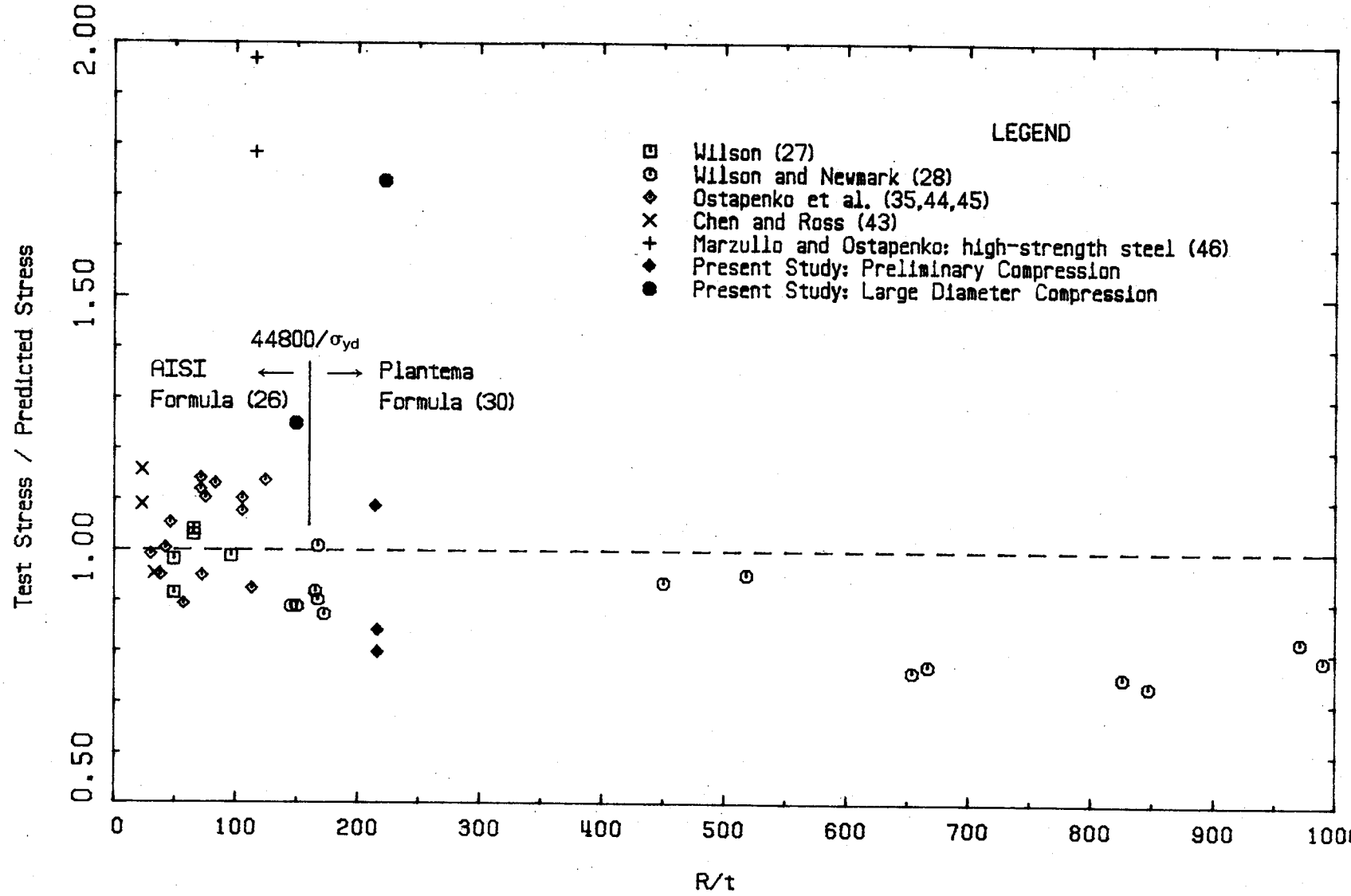

Figure 5.2 Comparison Between Measured and Predicted Buckling Stress (AISI-Plantema Formula)

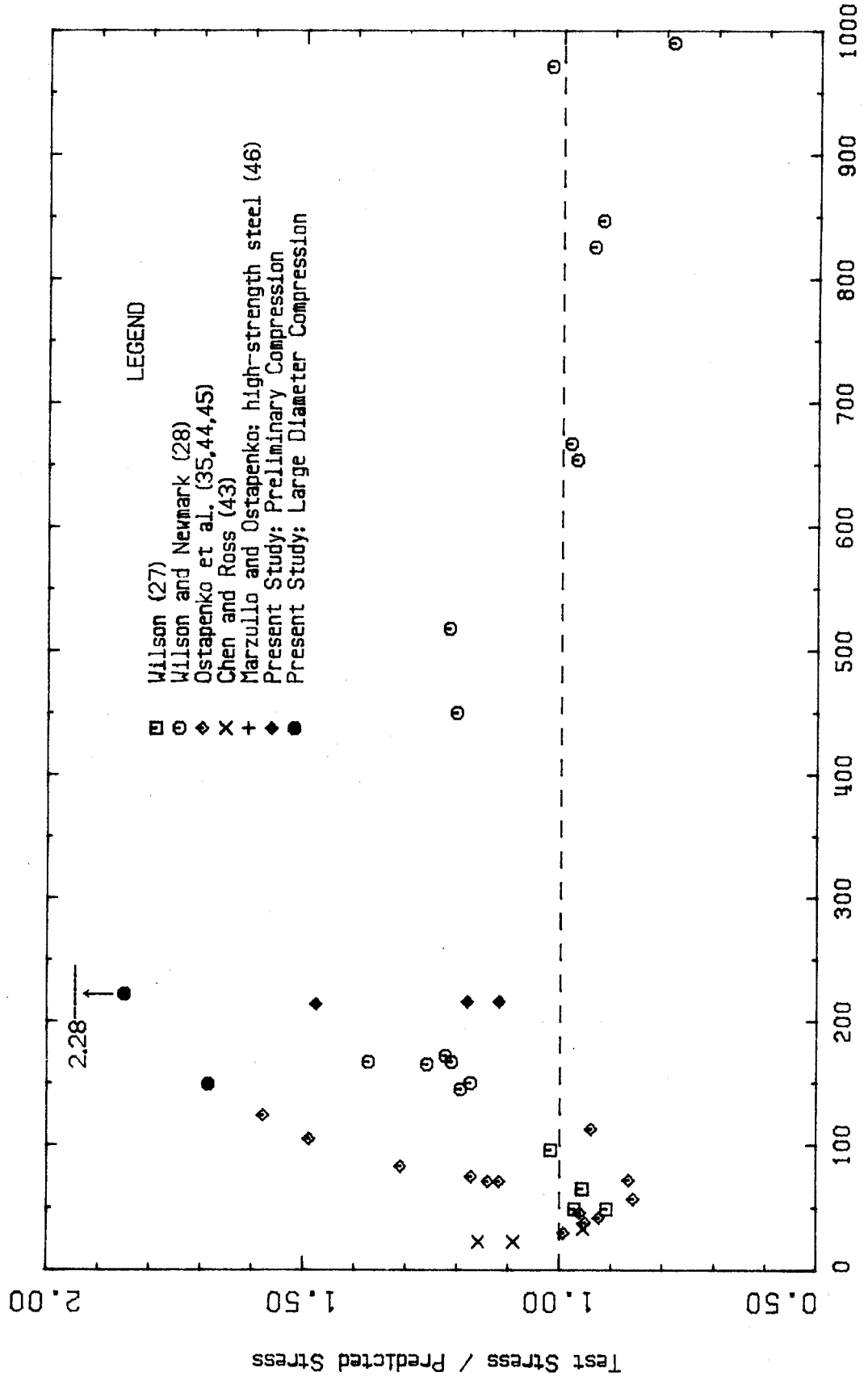

Figure 5.3 Comparison Between Measured and Predicted Buckling Stress (AWWA Formula)

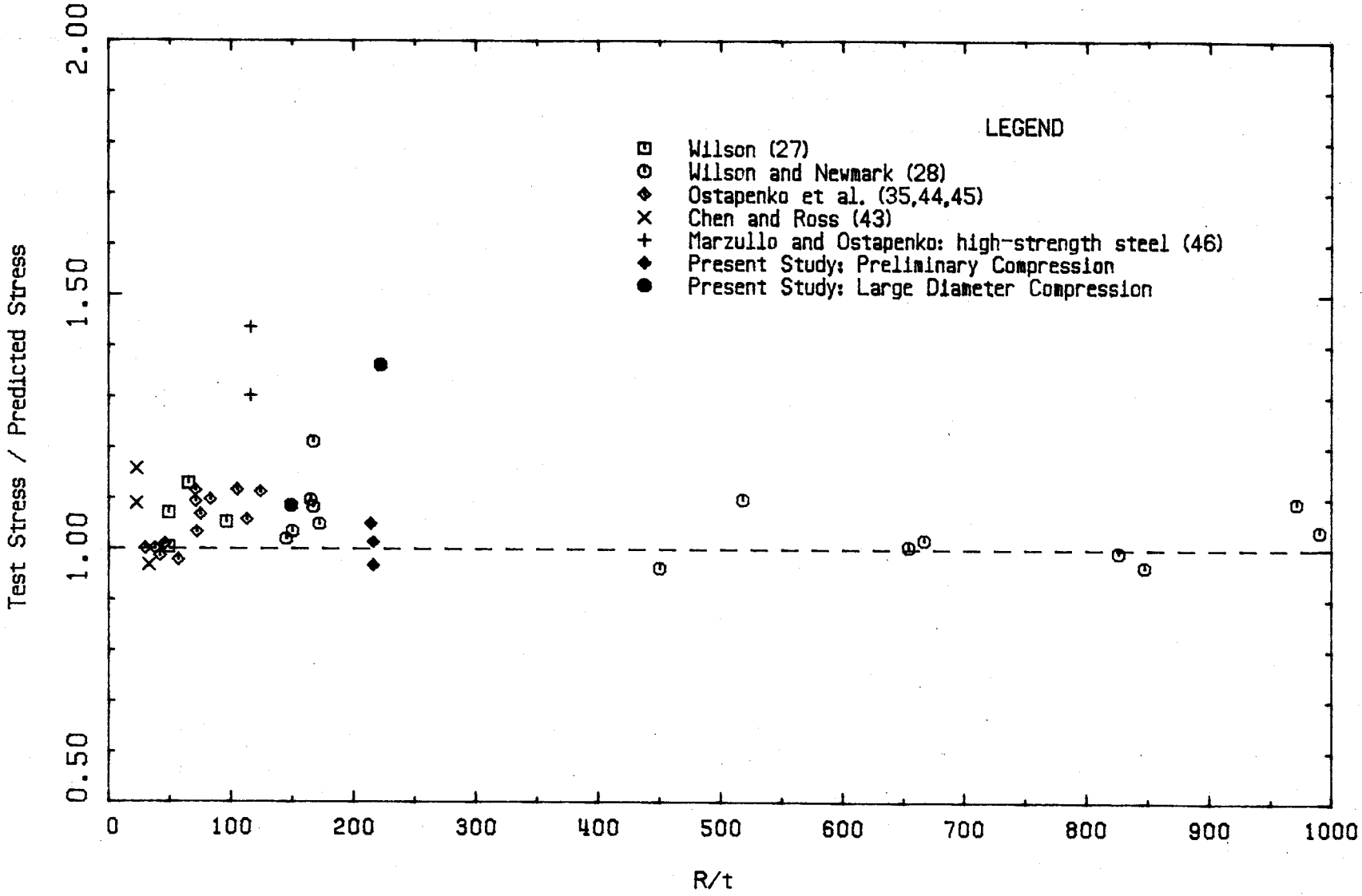

Figure 5.4 Comparison Between Measured and Predicted Buckling Stress (ASME Formula)

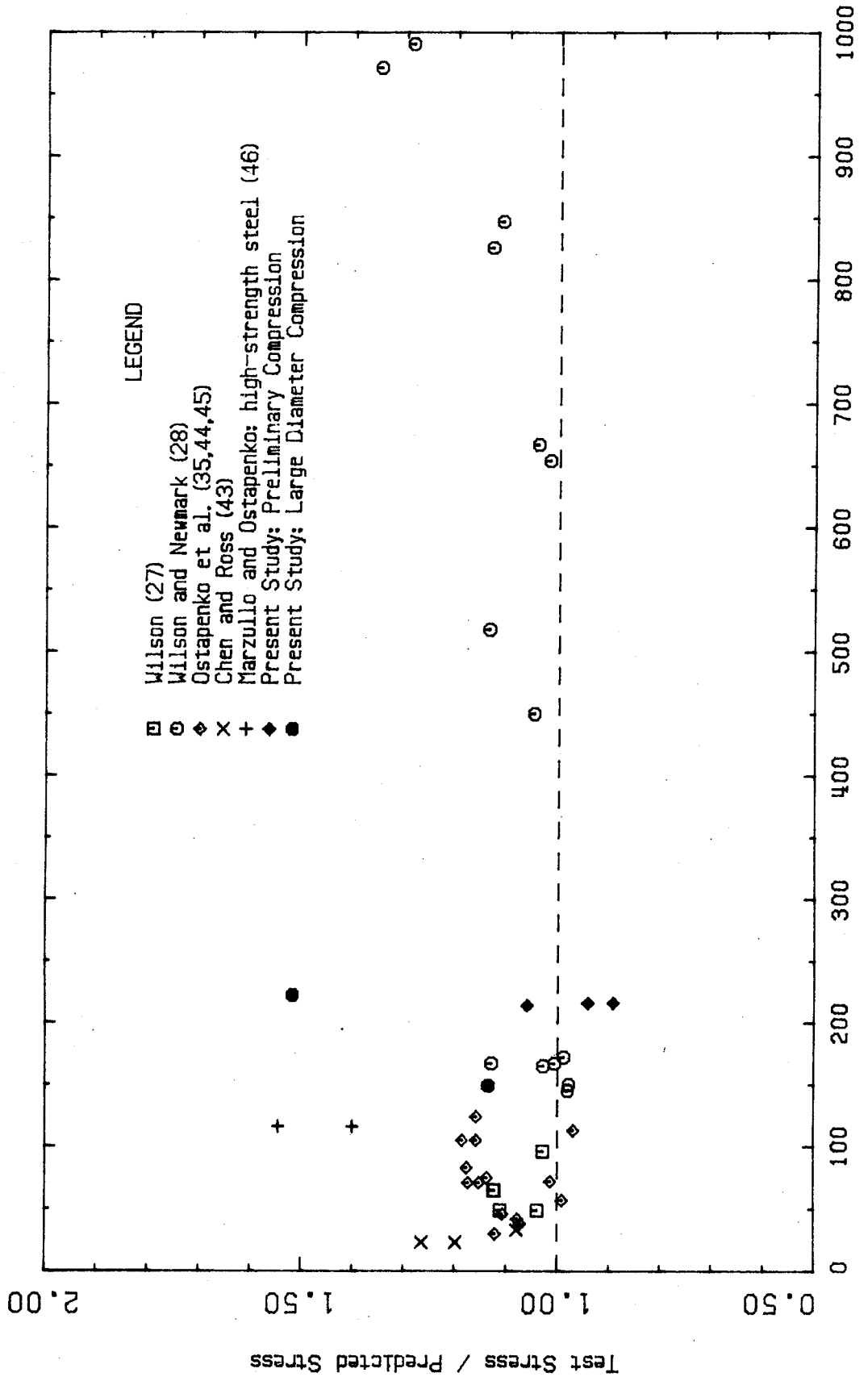

Figure 5.5 Comparison Between Measured and Predicted Buckling Stress (ECCS Formula)

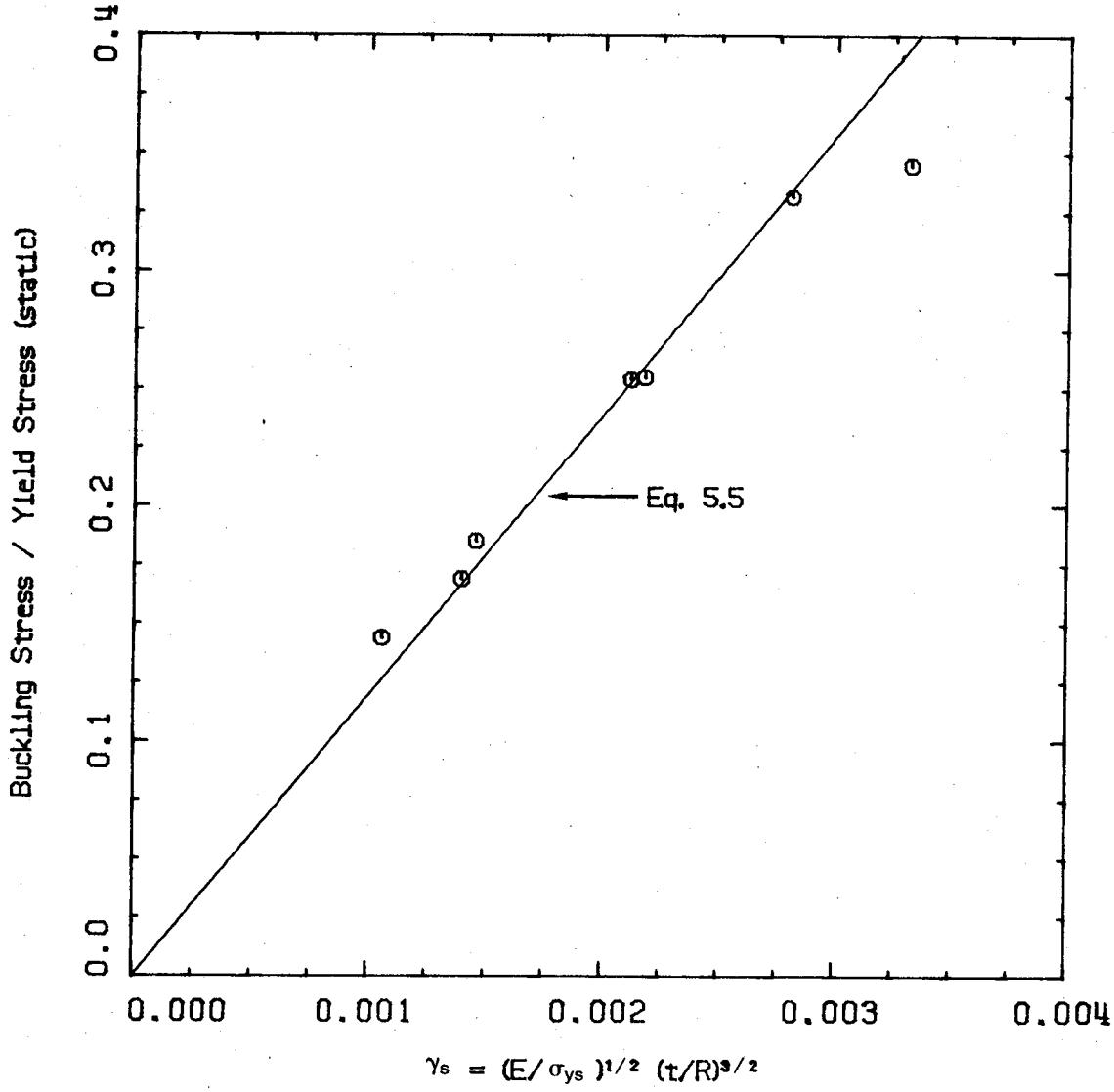

Figure 5.6 Best-Fit Line Through Test Results on Fabricated Cylinders Loaded in Axial Compression (Tests from Ref. 28)

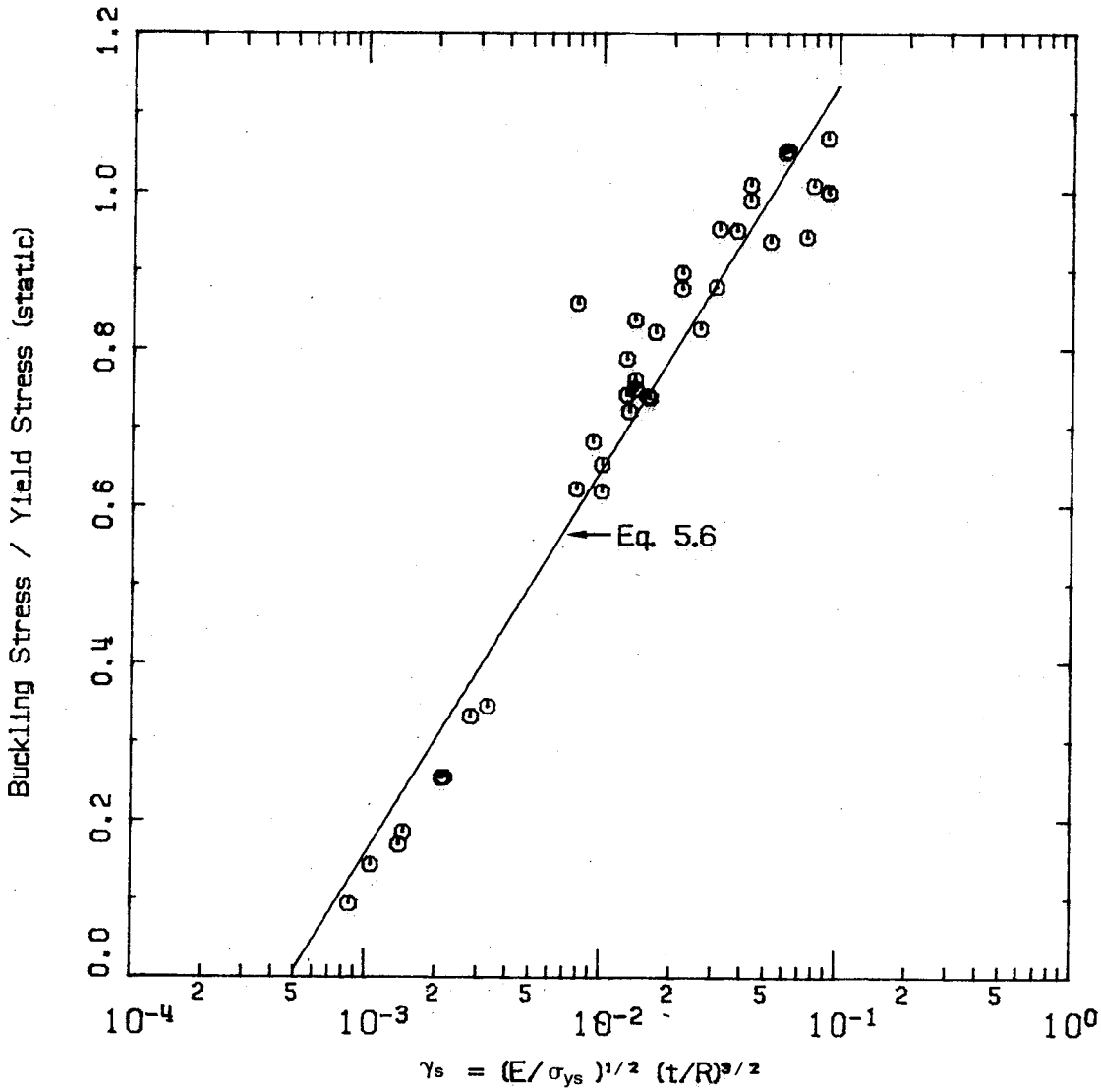

Figure 5.7 Semi-Log Best-Fit Line Through Test Results on Fabricated Cylinders Loaded in Axial Compression

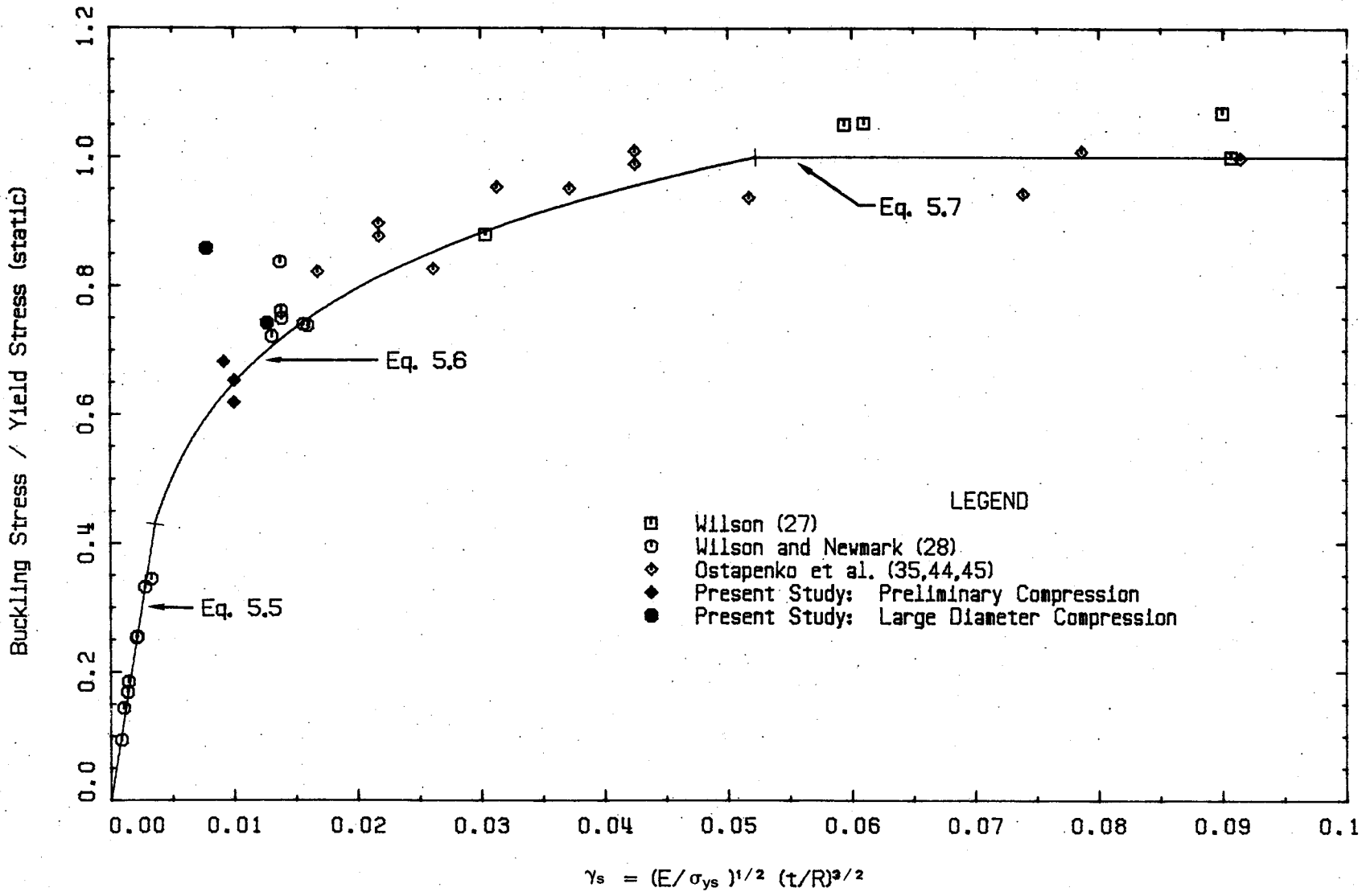

Figure 5.8 Proposed Local Buckling Ultimate Strength Curve for Axially Compressed Cylinders

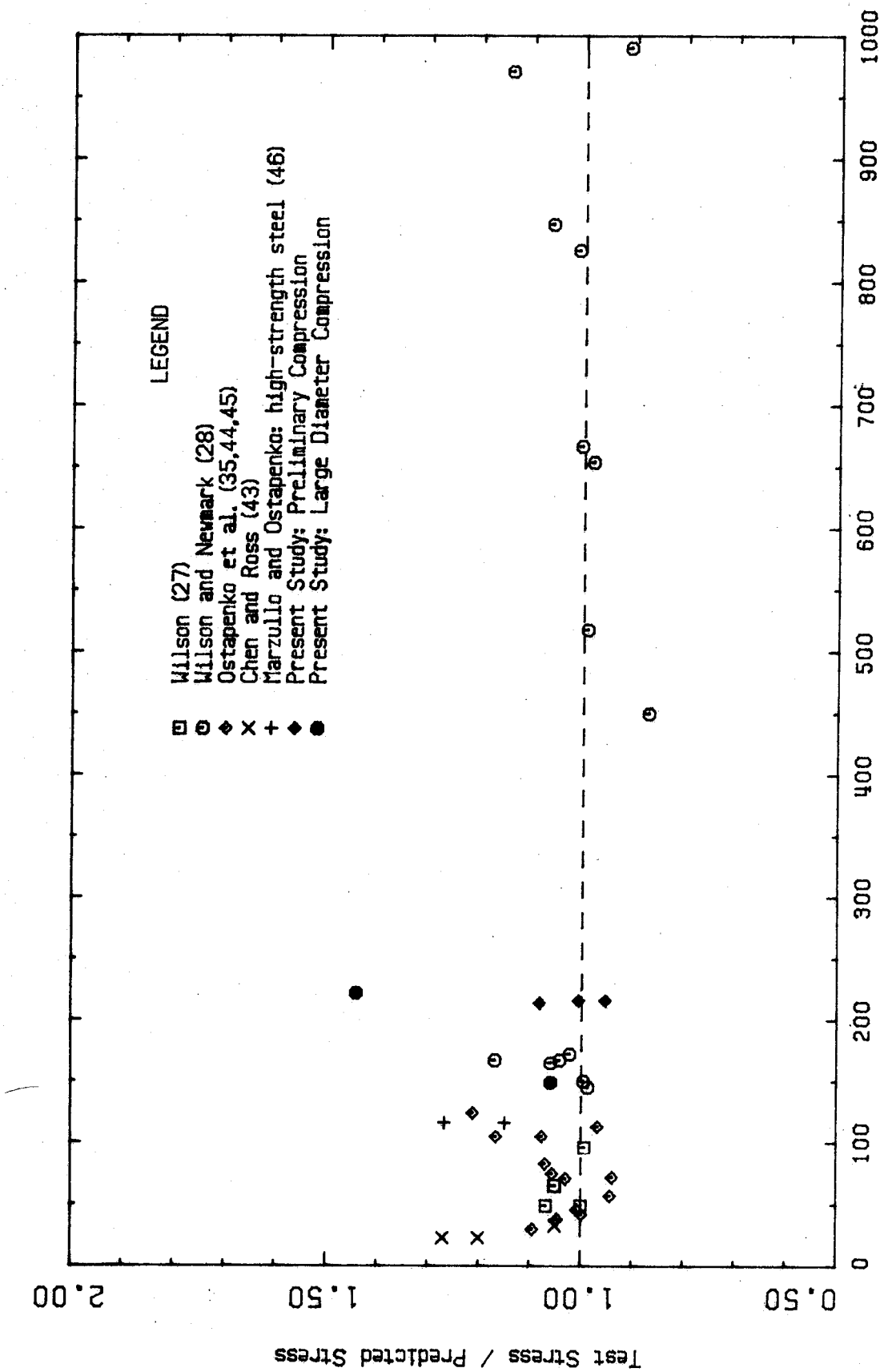

Figure 5.9 Comparison Between Measured and Predicted Buckling Stress (Proposed Formula)

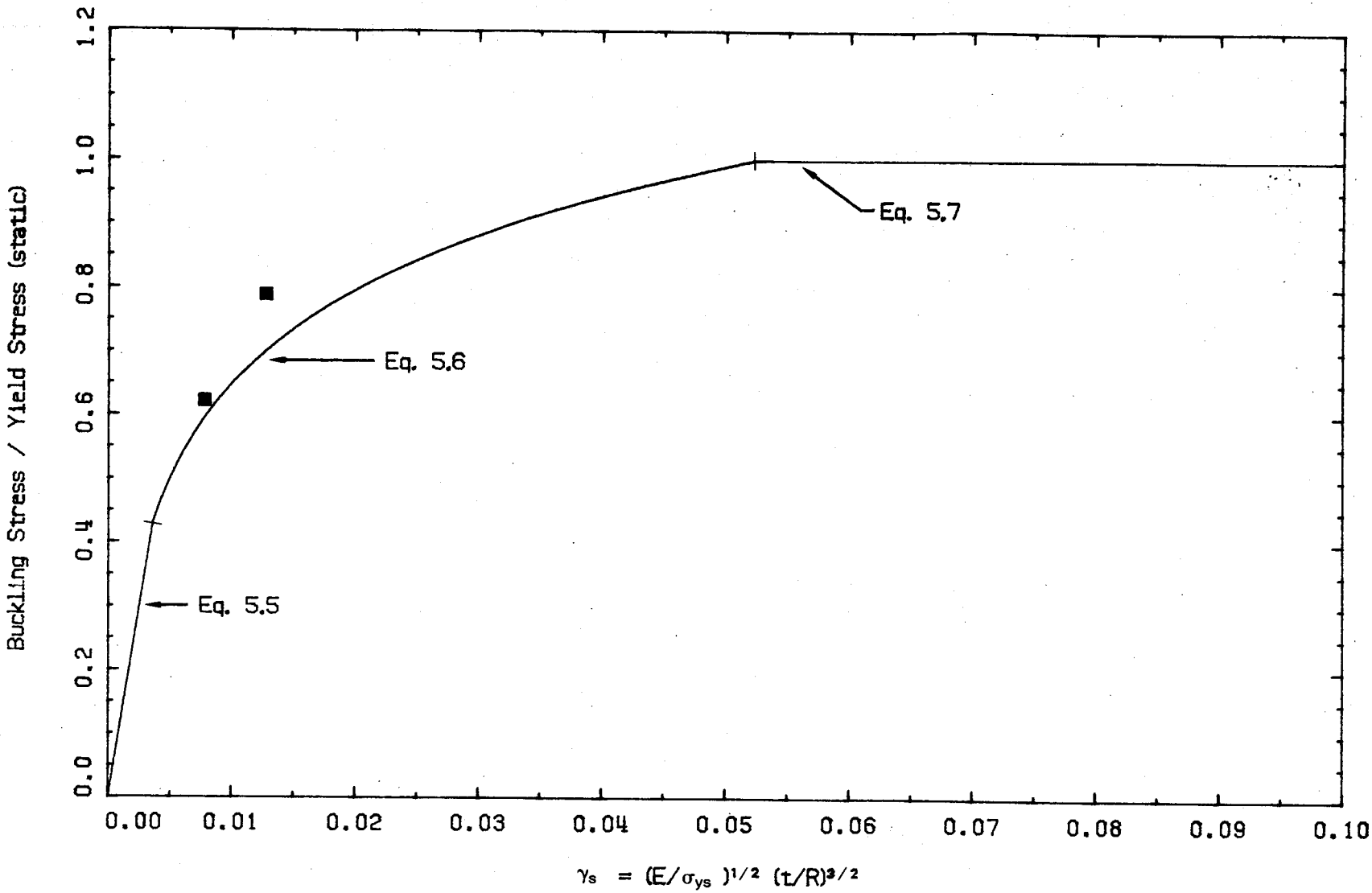

Figure 5.10 Bending Test Results in Relation to the Proposed Buckling Strength Curve

6. SUMMARY, CONCLUSIONS, AND RECOMMENDATIONS

6.1 Summary and Conclusions

This study was undertaken to investigate the local buckling behavior of thin-walled fabricated steel cylinders. Specifically, stability failure caused by uniform axial compression or by pure flexure at stress levels below the yield point was considered. The experimental phase of the study involved the testing of weld-fabricated tubes with cross-sectional geometries representative of large diameter tubular conveyor support systems.

Analysis of the test results obtained in this study together with a critical evaluation of the results obtained by others on fabricated cylinders has led to the following conclusions:

1. Cold forming and welding produces significant initial geometric imperfections. For the specimens tested herein, random local deviation amplitudes averaged 4% to 9% of the wall thickness; circumferential weld depression amplitudes averaged 20% to 60% of the wall thickness. Maximum imperfection amplitudes approached but did not exceed the cylinder wall thickness.
2. The observed effect of geometric imperfections on the buckling strength can be approximated by the imperfection theory of Koiter. Best agreement

between theory and experiment is achieved by assuming an imperfection amplitude equal to either the average or the root mean square of the measured values.

3. Nonhomogeneous material behavior, caused primarily by residual stresses, results in a proportional limit of about 60% of the static yield point for weld-fabricated, mild steel cylinders loaded in compression or bending.
4. The local buckling of fabricated steel tubes subjected to uniform axial compression occurs at a stress which is considerably less than the classical elastic buckling stress. For cylinders with wall thicknesses greater than approximately 6 mm, the existing ASME formula most closely approximates the actual buckling strength. Circumferential welds generally have a more pronounced detrimental effect on thinner-walled cylinders and, pending further investigation, the buckling strength of cylinders with wall thickness less than 6 mm is better approximated by the more conservative AWWA formula.
5. The proposed local buckling ultimate strength formula for compression is shown to accurately predict specimen behavior (for $t > 6$ mm), and is in a form particularly suited for design. In addition, it normalizes the test results over a wider range of

material yield strengths when compared with existing formulas.

6. The tests performed herein do not support an increased local buckling strength for flexurally loaded members. It is therefore reasonable to assume that the flexural buckling capacity of fabricated steel cylinders can be approximated on the basis of the test results for uniformly compressed cylinders.
7. The flexural buckling strength of large diameter weld-fabricated tubular conveyor galleries is best approximated by either the existing ASME formula or the proposed formula for axial compression.

6.2 Recommendations

1. Additional testing of fabricated tubular members loaded in pure flexure is required over a wide range of R/t ratios to conclusively establish the amount of strength increase afforded by a bending induced strain gradient.
2. Further experimental study is recommended to establish the effects of welding induced imperfections on the compressive and flexural buckling strength of cylinders with wall thicknesses less than about 6 mm.

REFERENCES

1. Lorenz, R., *Achsensymmetrische Vererrungen in Dünnwandigen Hohlzylinder*, Z. Ver. Deut. Ingen., Vol. 52, No. 43, 1908.

2. Timoshenko, S., *Einige Stabilitatsprobleme der Elastizitatstheorie*, Z. Math. Phys., Vol. 58, No. 4, 1910; later reference in: Theory of Elastic Stability, McGraw-Hill, New York, N. Y., 1961, pp. 457-485.

3. Southwell, R. V., *On the General Theory of Elastic Stability*, Phil. Trans. Roy. Soc. Lond., Series A, No. 213, 1914.

4. Flügge, W., *Die Stabilität der Kreiszylinderschale*, Ingen. Arch., Vol. 3, 1932; later reference in: Stresses in Shells, Springer-Verlag, New York, N. Y., 1973, pp. 452-459.

5. Donnell, L. H., *A New Theory for the Buckling of Thin Cylinders Under Axial Compression and Bending*, Trans. ASME, Vol. 56, 1934, AER-56-12.

6. Timoshenko, S., and Gere, J., Theory of Elastic Stability, McGraw-Hill, New York, N. Y., 1961, p. 465.

7. Esslinger, M., Geier, B., and Wood, J. G. M., *Some Complements to the ECCS Design Code Concerning Isotropic Cylinders*, Preliminary Report, Second International Coloquium on the Stability of Steel Structures, Liége, Belgium, 1977.

8. Timoshenko, S., and Gere, J., Theory of Elastic Stability, McGraw-Hill, New York, N. Y., 1961, pp. 482-485.

9. Seide, P., and Weingarten, V. I., *On the Buckling of Circular Cylindrical Shells and Other Thin Sections*, J. Appl. Mech., Vol. 28, No. 1, 1961.

10. Brazier, L. G., *On the Flexure of Thin Cylindrical Shells and Other Thin Sections*, Proc. Roy. Soc. Lond., Series A, Vol. 116, 1927.

11. Aksel'rad, E. L., *Refinement of the Upper Critical Load of Pipe Bending Taking into Account the Geometric Nonlinearity* (in Russian), Izvesiia, AN, SSSR, OTN, Mechanika, Masshinostroenie, No. 4, 1965.

12. Stephens, W. B., Starnes, J. H., and Almroth, B. O., *Collapse of Long Cylindrical Shells Under Combined Bending and Pressure Loads*, AIAA Paper No. 74-407, 1974.

13. National Aeronautics and Space Administration, *Buckling of Thin-Walled Circular Cylinders*, NASA Space Vehicle Design Criteria (Structures), NASA SP-8007, 1968.

14. Gerard, G., *Compressive and Torsional Buckling of Thin-Wall Cylinders in the Yield Region*, NACA TN-3726, 1956.

15. Almroth, B. O., *Influence of Edge Conditions on the Stability of Axially Compressed Cylindrical Shells*, AIAA J., Vol. 4, No. 1, 1966.

16. Batdorf, S. B., Schildcrout, M., and Stein, M., *Critical Stress of Thin-Walled Cylinders in Axial Compression*, NACA TN-1343, 1947.

17. von Kármán, T., and Tsien, H. S., *The Buckling of Thin Cylindrical Shells Under Axial Compression*, J. Aeron. Sci., Vol. 8, No. 8, 1941.

18. Koiter, W. T., *On The Stability of Elastic Eqiulibrium*, Thesis, Technical University Delft, Amsterdam, 1945; English translation: Air Force Flight Dynamics Laboratory, Air Force Systems Command, Wright-Patterson Air Force Base, Ohio, Technical Report AFFDL-TR-70-25, 1970.

19. Almroth, B. O., *Influence of Imperfections And Edge Constraint on the Buckling of Axially Compressed Cylinders*, NASA CR-432, 1966.

20. Tennyson, R. C., and Muggeridge, D. B., *Buckling of Axisymmetrically Imperfect Circular Cylindrical Shells Under Axial Compression*, AIAA J., Vol. 7, No. 11, 1966.

21. Arbocz, J., and Babcock, C. D., *Prediction of Buckling Loads Based on Experimentally Measured Initial Imperfections*, Buckling of Structures, edited by B. Budiansky, Springer-Verlag, New York, N. Y., 1976, pp. 295-296.

22. Arbocz, J., *The Effect of Initial Imperfections on Shell Stability*, Thin-Shell Structures, edited by Y. C. Fung and E. E. Sechler, Prentice-Hall, Englewood Cliffs, N. J., 1974.

23. Babcock, C. D., *Experiments in Shell Buckling*, Thin-Shell Structures, edited by Y. C. Fung and E. E. Sechler, Prentice-Hall, Englewood Cliffs, N. J., 1974.

24. Weingarten, V. I., Morgan, E. J., and Seide, P., *Elastic Stability of Thin-Walled Cylindrical and Conical Shells Under Axial Compression*, AIAA J., Vol. 3, No. 3, 1965.

25. Canadian Standards Association, *Cold Formed Steel Structural Members*, CSA Standard S136-1974, 1974.

26. American Iron and Steel Institute, *Specification for the Design of Light Gage Cold-Formed Steel Structural Members*, 1980.

27. Wilson, W. M., *Tests on Steel Columns*, Univ. Ill. Eng. Exp. Sta. Bull. No. 292, 1937.

28. Wilson, W. M., and Newmark, N. M., *The Strength of Thin Cylindrical Shells as Columns*, Univ. Ill. Eng. Exp. Sta. Bull. No. 255, 1933.

29. Structural Stability Research Council, Guide to Stability Design Criteria for Metal Structures, 3rd edition, edited by B. G. Johnston, John Wiley and Sons, New York, N. Y., 1976, pp. 278-281.

30. Plantema, F. J., *Collapsing Stresses of Circular Cylinders and Round Tubes*, Nat. Luchtvaartlaboratorium Rep. S.280, Amsterdam, 1946.

31. American Water Works Association, *AWWA Standard for Steel Tanks—Standpipes, Reservoirs, and Elevated Tanks—for Water Storage*, AWWA D100-79, 1979.

32. Miller, C. D., *Buckling of Axially Compressed Cylinders*, J. Stru. Div., ASCE, Vol. 103, No. ST3, Proc. Paper 12823, 1977.

33. Donnell, L. M., and Wan, C. C., *Effect of Imperfections on Buckling of Thin Cylinders and Columns Under Axial Compression*, J. Appl. Mech., Vol. 17, No. 1, 1950.

34. American Society of Mechanical Engineers, *Metal Containment Shell Buckling Design Methods*, Case N-284 of the ASME Boiler and Pressure Vessel Code, 1980.

35. Ostapenko, A., and Gunzelman, S. X., *Local Buckling of Tubular Steel Columns*, Methods of Structural Analysis, Vol. 2, ASCE, New York, N. Y., 1976.

36. Ross, D. A., and Chen, W. F., *The Axial Strength of Cylindrical Columns*, Offshore Technology Conference, Houston, Tex., May 3-6, 1976, OTC Paper 2683.

37. Structural Stability Research Council, Guide to Stability Design Criteria for Metal Structures, 3rd edition, edited by B. G. Johnston, John Wiley and Sons, New York, N. Y., 1976, p. 267.

38. European Convention for Construction Steelwork, *Buckling of Shells*, Recommendations of Task Group T8-79-37, Proposed Rules R4.6, 1979.

39. American Society for Testing and Materials, *Mechanical Testing of Steel Products*, ASTM A370-77, 1981.

40. Tennyson, R. C., Muggeridge, D. B., and Caswell, R. D., *Buckling of Circular Cylindrical Shells Having Axisymmetric Imperfection Distibutions*, AIAA J., Vol. 9, No. 5, 1971.

41. American Petroleum Institute, *Specification for Fabricated Structural Pipe*, API Spec. 2B, Third Edition, 1977.

42. Rao, N. R. N., Lohrman, M., and Tall, L., *Effect of Strain Rate on the Yield Stress of Structural Steel*, J. Mat., ASTM, Vol. 1, No. 1, 1966.

43. Chen, W. F., and Ross, D. A., *The Strength of Axially Loaded Tubular Columns*, Rep. No. 406.7, Fritz Eng. Lab., Lehigh Univ., Bethlehem, Pa., 1978.

44. Gunzelman, S. X., and Ostapenko, A., *Local Buckling Tests on Three Steel Large-Diameter Tubular Columns*, Rep. No. 393.8, Fritz Eng. Lab., Lehigh Univ., Bethlehem, Pa., 1977.

45. Ostapenko, A., and Grimm, D. F., *Local Buckling of Cylindrical Tubular Columns Made of A36 Steel*, Rep. No. 450.7, Fritz Eng. Lab., Lehigh Univ., Bethlehem, Pa., 1980.

46. Marzullo, M. A., and Ostapenko, A., *Tests on Two High-Strength Short Tubular Columns*, Rep. No. 406.10, Fritz Eng. Lab., Lehigh Univ., Bethlehem, Pa., 1977.

47. Edlund, Bo L. O., *Buckling of Axially Compressed Thin-Walled Cylindrical Shells with Asymmetric Imperfections*, Preliminary Report, Second International Coloquium on the Stability of Steel Structes, Liége, Belgium, 1977.

48. von Kármán, T., *The Strength of Thin Plates in Compression*, Trans. ASME, Vol. 54, 1932, APM-54-5.

49. Sherman, D. R., *Tests of Circular Steel Tubes in Bending*, J. Stru. Div., ASCE, Vol. 102, No. ST11, Proc. Paper 12568, 1976.

50. Allen, D., discussion of *Tests on Circular Steel Tubes in Bending*, by D. R. Sherman, J. Stru. Div., ASCE, Vol. 103, No. ST7, Proc. Paper 13111, 1977.

RECENT STRUCTURAL ENGINEERING REPORTS

Department of Civil Engineering

University of Alberta

74. *An Effective Uniaxial Tensile Stress-Strain Relationship for Prestressed Concrete* by L. Chitnuyanondh, S. Rizkalla, D.W. Murray and J.G. MacGregor, February 1979.

75. *Interaction Diagrams for Reinforced Masonry* by C. Feeg and J. Warwaruk, April 1979.

76. *Effects of Reinforcement Detailing for Concrete Masonry Columns* by C. Feeg, J. Longworth and J. Warwaruk, May 1979.

77. *Interaction of Concrete Masonry Bearing Walls and Concrete Floor Slabs* by N. Ferguson, J. Wongworth and J. Warwaruk, May 1979.

78. *Analysis of Prestressed Concrete Wall Segments* by B.D.P. Koziak and D.W. Murray, June 1979.

79. *Fatigue Strength of Welded Steel Elements* by M.P. Comeau and G.L. Kulak, October 1979.

80. *Leakage Tests of Wall Segments of Reactor Containments* by S.K. Rizkalla, S.H. Simmonds and J.G. MacGregor, October 1979.

81. *Tests of Wall Segments from Reactor Containments* by S.H. Simmonds, S.K. Rizkalla and J.G. MacGregor, October 1979.

82. *Cracking of Reinforced and Prestressed Concrete Wall Segments* by J.G. MacGregor, S.K. Rizkalla and S.H. Simmonds, October 1979.

83. *Inelastic Behavior of Multistory Steel Frames* by M. El Zanaty, D.W. Murray and R. Bjorhovde, April 1980.

84. *Finite Element Programs for Frame Analysis* by M. El Zanaty and D.W. Murray, April 1980.

85. *Test of a Prestressed Concrete Secondary Containment Structure* by J.G. MacGregor, S.H. Simmonds and S.H. Rizkalla, April 1980.

86. *An Inelastic Analysis of the Gentilly-2 Secondary Containment Structure* by D.W. Murray, C. Wong, S.H. Simmonds and J.G. MacGregor, April 1980.

87. *Nonlinear Analysis of Axisymmetric Reinforced Concrete Structures* by A.A. Elwi and D.W. Murray, May 1980.

88. *Behavior of Prestressed Concrete Containment Structures - A Summary of Findings* by J.G. MacGregor, D.W. Murray, S.H. Simmonds, April 1980.

89. *Deflection of Composite Beams at Service Load* by L. Samantaraya and J. Longworth, June 1980.

90. *Analysis and Design of Stub-Girders* by T.J.E. Zimmerman and R. Bjorhovde, August 1980.

91. *An Investigation of Reinforced Concrete Block Masonry Columns* by G.R. Sturgeon, J. Longworth and J. Warwaruk, September 1980.

92. *An Investigation of Concrete Masonry Wall and Concrete Slab Interaction* by R.M. Pacholok, J. Warwaruk and J. Longworth, October 1980.

93. *FEPARCS5 - A Finite Element Program for the Analysis of Axisymmetric Reinforced Concrete Structures - Users Manual* by A. Elwi and D.W. Murray, November 1980.

94. *Plastic Design of Reinforced Concrete Slabs* by D.M. Rogowsky and S.H. Simmonds, November 1980.

95. *Local Buckling of W Shapes Used as Columns, Beams, and Beam-Columns* by J.L. Dawe and G.L. Kulak, March 1981.

96. *Dynamic Response of Bridge Piers to Ice Forces* by E.W. Gordon and C.J. Montgomery, May 1981.

97. *Full-Scale Test of a Composite Truss* by R. Bjorhovde, June 1981.

98. *Design Methods for Steel Box-Girder Support Diaphragms* by R.J. Ramsay and R. Bjorhovde, July 1981.

99. *Behavior of Restrained Masonry Beams* by R. Lee, J. Longworth and J. Warwaruk, October 1981.

100. *Stiffened Plate Analysis by the Hybrid Stress Finite Element Method* by M.M. Hrabok and T.M. Hrudey, October 1981.

101. *Hybslab - A Finite Element Program for Stiffened Plate Analysis* by M.M. Hrabok and T.M. Hrudey, November 1981.

102. *Fatigue Strength of Trusses Made From Rectangular Hollow Sections* by R.B. Ogle and G.L. Kulak, November 1981.

103. *Local Buckling of Thin-Walled Tubular Steel Members* by M.J. Stephens, G.L. Kulak and C.J. Montgomery, February 1982.

104. *Test Methods for Evaluating Mechanical Properties of Waferboard: A Preliminary Study* by M. MacIntosh and J. Longworth, May 1982.